

The Most Metal-poor Stars in the Inner Bulge*

HENRIQUE REGGIANI,¹ KEVIN C. SCHLAUFMAN,¹ ANDREW R. CASEY,^{2,3} AND ALEXANDER P. JI^{4,†}

¹*Department of Physics and Astronomy, Johns Hopkins University, 3400 N Charles St., Baltimore, MD 21218, USA*

²*School of Physics & Astronomy, Monash University, Wellington Road, Clayton 3800, Victoria, Australia*

³*ARC Centre of Excellence for All Sky Astrophysics in 3 Dimensions (ASTRO 3D), Canberra, ACT 2611, Australia*

⁴*The Observatories of the Carnegie Institution for Science, 813 Santa Barbara St., Pasadena, CA 91101, USA*

(Received July 6, 2020; Revised July 24, 2020; Accepted July 24, 2020)

Submitted to AAS Journals

ABSTRACT

The bulge is the oldest component of the Milky Way. Since numerous simulations of Milky Way formation have predicted that the oldest stars at a given metallicity are found on tightly bound orbits, the Galaxy’s oldest stars are likely metal-poor stars in the inner bulge with small apocenters (i.e., $R_{\text{apo}} \lesssim 4$ kpc). In the past, stars with these properties have been impossible to find due to extreme reddening and extinction along the line of sight to the inner bulge. We have used the mid-infrared metal-poor star selection of [Schlaufman & Casey \(2014\)](#) on Spitzer/GLIMPSE data to overcome these problems and target candidate inner bulge metal-poor giants for moderate-resolution spectroscopy with AAT/AAOmega. We used those data to select three confirmed metal-poor giants ($[\text{Fe}/\text{H}] = -3.15, -2.56, -2.03$) for follow-up high-resolution Magellan/MIKE spectroscopy. A comprehensive orbit analysis using Gaia DR2 astrometry and our measured radial velocities confirms that these stars are tightly bound inner bulge stars. We determine the elemental abundances of each star and find high titanium and iron-peak abundances relative to iron in our most metal-poor star. We propose that the distinct abundance signature we detect is a product of nucleosynthesis in the Chandrasekhar-mass thermonuclear supernova of a CO white dwarf accreting from a helium star with a delay time of about 10 Myr. Even though chemical evolution is expected to occur quickly in the bulge, the intense star formation in the core of the nascent Milky Way was apparently able to produce at least one Chandrasekhar-mass thermonuclear supernova progenitor before chemical evolution advanced beyond $[\text{Fe}/\text{H}] \sim -3$.

Keywords: Galactic bulge (2041); Milky Way dynamics (1051); Milky Way formation (1053); Population II stars (1284); Stellar abundances (1577); Type Ia supernovae (1728)

1. INTRODUCTION

Since galaxies form from the inside-out, the bulge is the oldest major component of the Milky Way. While there are at least six physical processes that may have contributed to the growth of the Milky Way’s bulge (e.g., [Barbuy et al. 2018](#)), it is statistically implausible that

the earliest stage of Milky Way formation failed to contribute to the bulge’s stellar population at some level. Indeed, numerical simulations of Milky Way-analog formation have consistently shown that the metal-poor stars in the inner few kpc of a Milky Way-like galaxy are often the oldest stars in the dark matter halo hosting the galaxy.¹ At the same time, the early chemical evolution of the bulge is expected to differ significantly

Corresponding author: Henrique Reggiani
hreggiani@jhu.edu

* This paper includes data gathered with the 6.5-meter Magellan Telescopes located at Las Campanas Observatory, Chile.

† Hubble Fellow

¹ See for example [Diemand et al. \(2005\)](#), [Scannapieco et al. \(2006\)](#), [Brook et al. \(2007\)](#), [Salvadori et al. \(2010\)](#), [Gao et al. \(2010\)](#), [Tumlinson \(2010\)](#), [Ishiyama et al. \(2016\)](#), [Starkeburg et al. \(2017\)](#), [Griffen et al. \(2018\)](#), and [Sharma et al. \(2018\)](#)

from that of the halo and surviving dwarf galaxies (e.g., Kobayashi et al. 2006). For these reasons, the exploration of this first stage of Milky Way formation using the chemical abundances of ancient metal-poor stars in the inner Galaxy has long been a goal of Galactic archaeology.

Some of the expected differences in the chemical evolution of the bulge and halo have already been observed (e.g., Kobayashi et al. 2006; Cunha & Smith 2006; Johnson et al. 2012; Bensby et al. 2017; Gargiulo et al. 2017; Barbuy et al. 2018). The star formation rates in the event (or events) that lead to the formation of Milky Way’s “classical bulge” component are thought to have been very high. This intense star formation in a metal-poor environment would have produced many otherwise uncommon stellar systems, perhaps including the progenitors of relatively rare classes of supernovae (e.g., hypernovae, spinstars, thermonuclear supernovae on core-collapse supernovae timescales, etc.). The existence of metal-poor stars in the inner bulge despite this intense star formation requires the accretion of unenriched gas on short timescales as expected in the denser and more gas-rich $z \gtrsim 2$ Universe. Both of these differences between the bulge and the halo/surviving dwarf galaxies—frequent contributions from rare supernovae and the signature of ongoing accretion of unenriched gas—should be apparent in comparisons of the detailed elemental abundances of the most metal-poor stars in the inner bulge, halo, and surviving dwarf galaxies.

While metal-poor stars in the inner Galaxy were historically difficult to separate from the much more numerous metal-rich stars in the bulge, significant progress has been made in the last few years. Several groups have discovered metal-poor giants in the outer bulge photometrically using ultraviolet or mid-infrared photometry or spectroscopically in multiplexed surveys (e.g., García Pérez et al. 2013; Ness et al. 2013; Casey & Schlafman 2015; Howes et al. 2015, 2016; Lamb et al. 2017; Lucey et al. 2019; Arentsen et al. 2020). In spite of this recent progress in the outer bulge, it has been impossible to study in detail or even find metal-poor stars with $[\text{Fe}/\text{H}] \lesssim -2.0$ in the inner bulge (i.e., $|l, b| \lesssim 4^\circ$) due to the extreme extinction and reddening in that direction.

In this paper, we have used the infrared-only metal-poor star selection of Schlafman & Casey (2014) to discover the most metal-poor stars known in the inner bulge. Follow-up high-resolution optical spectroscopy has revealed that at $[\text{Fe}/\text{H}] \sim -3$, the inner bulge has high silicon and iron-peak abundances relative to iron when compared to giant stars in the halo or surviving dwarf galaxies. We attribute these differences to the occurrence of at least one Chandrasekhar-mass thermonu-

clear supernova that occurred early in the bulge’s chemical evolution on a timescale comparable to core-collapse supernovae. We outline our sample selection and observations in Section 2. We describe our analyses of these data in Section 3 and report the chemical abundances we infer in Section 4. We discuss the implications of our findings in Section 5 and summarize our findings in Section 6.

2. SAMPLE SELECTION AND OBSERVATIONS

As input to our candidate selection process we used the Two Micron All Sky Survey (2MASS) All-Sky Point Source Catalog (PSC) (Skrutskie et al. 2006) combined with Spitzer/IRAC Galactic Legacy Infrared Mid-Plane Survey Extraordinaire (GLIMPSE) II and GLIMPSE 3D catalogs (Benjamin et al. 2003; Churchwell et al. 2009). We dereddened and extinction-corrected these photometric catalogs with the bulge-specific reddening maps from Gonzalez et al. (2011, 2012) assuming a Nishiyama et al. (2009) extinction law. We excluded all stars with non-zero data quality flags (indicating a possible data quality issue), neighbors within $2''$, or extinction-corrected apparent 2MASS J -band magnitudes $J_0 \geq 12.5$. The latter cut ensured that we focused our attention on giant stars on the near side of the bulge. We then applied the infrared-only “v1” metal-poor star selection from Schlafman & Casey (2014) to the dereddened and extinction-corrected 2MASS and Spitzer/IRAC photometry to generate our initial candidate list. The cuts described above resulted in a sample of 10,915 candidate metal-poor giants with $-10 \leq l \leq +10$ and $-5 \leq b \leq +5$. To help prioritize spectroscopic follow-up, we also estimated extinction-corrected I -band magnitudes assuming a typical $(I - J)_0 = 0.8$ color for metal-poor giants bright enough to have $J_0 \lesssim 12.5$ at 8 kpc.

We observed several thousand of these candidate inner bulge metal-poor giants using the Anglo-Australian Telescope’s (AAT) AAOmega multiobject spectrograph fed by the 2 Degree Field (2dF) robotic fibre positioner. We used the 580V and 1700D gratings in the blue and red arms of the spectrograph, providing spectral resolution $R \approx 1,300$ between 370 and 580 nm in the blue and $R \approx 10,000$ between 845 and 900 nm in the red. We reduced these data using the standard `2dfdr` pipeline.² We estimated spectroscopic stellar parameters effective temperature T_{eff} , surface gravity $\log g$, and metallicity $[\text{Fe}/\text{H}]$ using the `sick` package (Casey 2016).³ We then selected the giants 2MASS J172452.74-281459.4,

² <https://www.aao.gov.au/science/software/2dfdr>

³ <https://github.com/andycasey/sick>

2MASS J175228.08-320947.6, and 2MASS J175836.79-313707.6 for high-resolution follow-up based on their low α -enhanced metallicities and bright apparent magnitudes. We plot the locations of these three stars on the Gaia DR2 all-sky image of the Galaxy in Figure 1.

We followed up these three giants with the Magellan Inamori Kyocera Echelle (MIKE) spectrograph on the Magellan Clay Telescope at Las Campanas Observatory (Bernstein et al. 2003; Shectman & Johns 2003). We used either the 0".7 or 1".0 slits and the standard blue and red grating azimuths, yielding spectra between 335 nm and 950 nm with resolution $R \approx 40,000/28,000$ in the blue and $R \approx 31,000/22,000$ in the red for the 0".7/1".0 slits. We collected all calibration data (e.g., bias, quartz & “milky” flat field, and ThAr lamp frames) in the afternoon before each night of observations. We present a log of these observations in Table 1. We reduced the raw spectra and calibration frames using the CarPy⁴ software package (Kelson et al. 2000; Kelson 2003; Kelson et al. 2014). We used iSpec⁵ (Blanco-Cuaresma et al. 2014; Blanco-Cuaresma 2019) to calculate radial velocities and barycentric corrections and normalized individual orders using IRAF⁶ (Tody 1986, 1993).

The extreme extinction and reddening towards the inner bulge strongly affected the signal-to-noise ratio S/N of our spectra blueward of 600 nm. At 400 nm near the Ca II H and K lines, our spectra have $S/N \approx 3/\text{pixel}$. At 520 nm near the Mg I *b* triplet our spectra have $S/N \approx 10/\text{pixel}$, while at 660 nm near H α our spectra have $S/N \approx 60/\text{pixel}$. Near the near-infrared Ca II triplet at 850 nm, our spectra have $S/N \approx 120/\text{pixel}$. We therefore focused our absorption line measurements on the long wavelength portions of our spectra.

3. STELLAR PROPERTIES

3.1. Stellar Parameters

We used the `isochrones`⁷ (Morton 2015) package to estimate T_{eff} and $\log g$ of each star using as inputs their:

1. g and r magnitudes and associated uncertainties from Data Release (DR) 1.1 of the SkyMapper Southern Sky Survey (Wolf et al. 2018);
2. J , H , and K_s magnitudes and associated uncertainties from the 2MASS PSC (Skrutskie et al. 2006);
3. $W1$, $W2$, and $W3$ magnitudes and associated uncertainties from the Wide-field Infrared Survey Explorer (WISE) AllWISE Source Catalog (Wright et al. 2010; Mainzer et al. 2011);
4. prior-informed distance estimates from Bailer-Jones et al. (2018) based on Gaia DR2 astrometry (Gaia Collaboration et al. 2016, 2018; Arenou et al. 2018; Hambly et al. 2018; Lindegren et al. 2018; Luri et al. 2018).

We used `isochrones` to fit the Dartmouth Stellar Evolution Database (Dotter et al. 2007, 2008) library generated with the Dartmouth Stellar Evolution Program (DSEP) to these observables using MultiNest⁸ (Feroz & Hobson 2008; Feroz et al. 2009, 2019). We restricted the Dartmouth library to α -enhanced composition $[\alpha/\text{Fe}] = +0.4$, stellar age τ in the range $10.0 \text{ Gyr} \leq \tau \leq 13.721 \text{ Gyr}$, and extinction A_V in the range $2.0 \text{ mag} \leq A_V \leq 5.0 \text{ mag}$. For each star, we initially assumed the values $T_{\text{eff}} = 4750 \pm 250 \text{ K}$, $\log g = 2 \pm 1$, $[\text{Fe}/\text{H}] = -3.0 \pm 1.0$ for the likelihood calculation. We limited distances d considered to the range suggested by Bailer-Jones et al. (2018). We plot the locations of all three stars relative to isochrones in $J - K_s$ versus K_s color-magnitude diagrams in Figure 2 and give the resulting isochrone-inferred parameters T_{eff} , $\log g$, A_V , τ , stellar luminosity L_* , stellar mass M_* , and isochrone distance d_{iso} in Table 2. This approach is analogous to the StarHorse technique from Queiroz et al. (2018, 2020).

⁴ <http://code.obs.carnegiescience.edu/mike>

⁵ <https://www.blancocuaresma.com/s/iSpec>

⁶ <https://iraf-community.github.io/>

⁷ <https://github.com/timothydmorton/isochrones>

⁸ <https://ccpforge.cse.rl.ac.uk/gf/project/multinest/>

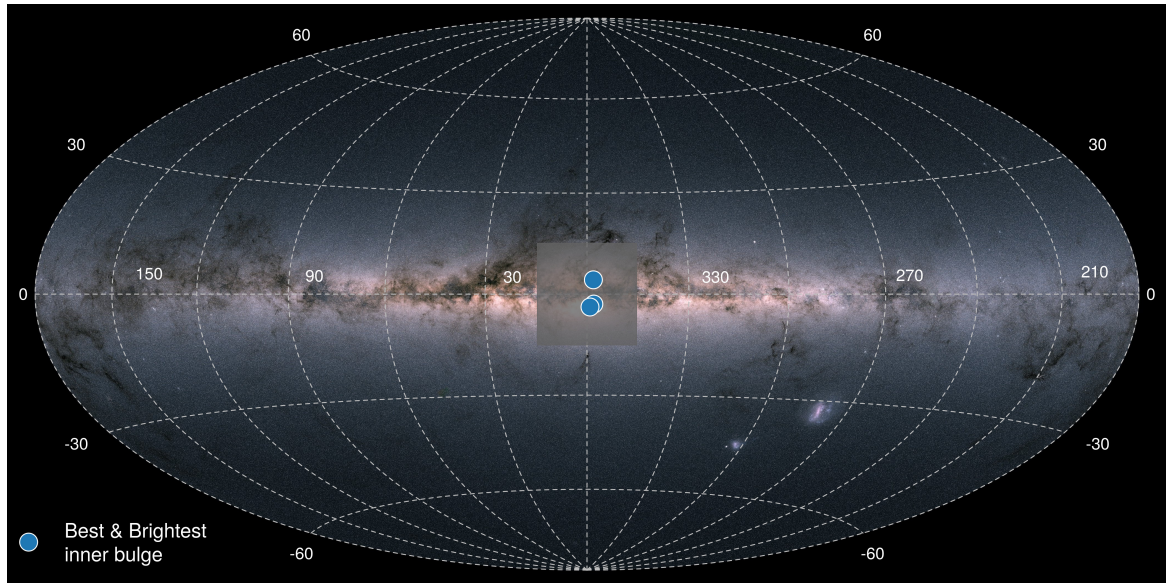


Figure 1. Gaia DR2 image of the Milky Way. We indicate the locations of the metal-poor inner bulge giants 2MASS J172452.74-281459.4, 2MASS J175228.08-320947.6, and 2MASS J175836.79-313707.6 as blue points. The shaded rectangle indicates the region in which [Tumlinson \(2010\)](#) suggest that more than ten percent of stars with $[\text{Fe}/\text{H}] \leq -3$ formed at a time equivalent to $z > 15$, or more than 13.45 Gyr in the past ([Wright 2006](#)).

Table 1. Log of Magellan/MIKE Observations

Star	UT Date	Start	End	Slit Width	Exposure Time	RV
					(s)	(km s^{-1})
J172452.74-281459.4	06/29/2017	04:21:29	04:32:29	1''0	660	+9.23
J175228.08-320947.6	06/29/2017	04:34:37	04:54:37	1''0	1200	-62.52
J175228.08-320947.6	07/02/2017	03:52:14	04:38:38	0''7	2700	-63.98
J175836.79-313707.6	06/29/2017	02:56:51	04:19:21	1''0	4800	-196.42
J175836.79-313707.6	06/29/2017	04:56:40	05:26:40	1''0	1800	-196.42

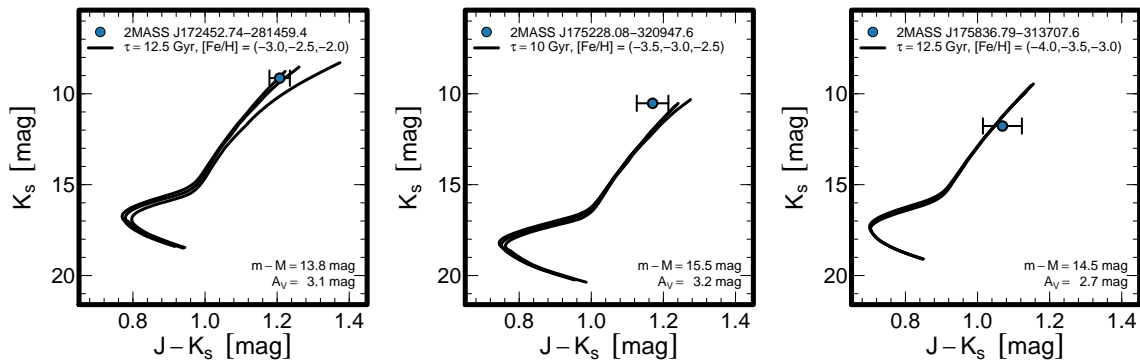


Figure 2. Locations of the three stars in our sample relative to Dartmouth isochrones with the indicated parameters.

Table 2. Stellar Properties and Adopted Parameters

Property	J172452.74-281459.4	J175228.08-320947.6	J175836.79-313707.6	Units
Astrometric and Photometric Properties				
Gaia DR2 Source ID	4059924905887808128	4043617705316006272	4043987927121580928	
Gaia DR2 R.A. α (J2000)	17 24 52.7503	17 52 28.0857	17 58 36.7952	h m s
Gaia DR2 decl. δ (J2000)	-28 14 59.287	-32 09 47.652	-31 37 07.674	d m s
Gaia DR2 galactic longitude l (J2000)	358.1186	357.9902	359.1173	degrees
Gaia DR2 galactic latitude b (J2000)	4.2026	-2.9241	-3.7794	degrees
Gaia DR2 proper motion (J2000) $\mu_\alpha \cos \delta$	-2.72 ± 0.10	-0.84 ± 0.09	-0.81 ± 0.16	mas yr $^{-1}$
Gaia DR2 proper motion (J2000) μ_δ	-10.28 ± 0.07	-3.12 ± 0.08	-7.65 ± 0.13	mas yr $^{-1}$
Gaia DR2 parallax π (J2000)	0.22 ± 0.06	0.04 ± 0.06	0.15 ± 0.07	mas
SkyMapper g	15.560 ± 0.010	16.743 ± 0.023	17.261 ± 0.027	AB mag
SkyMapper r	...	15.384 ± 0.007	15.967 ± 0.007	AB mag
Gaia DR2 G	13.75 ± 0.002	14.95 ± 0.002	15.70 ± 0.002	Vega mag
2MASS J	10.346 ± 0.019	11.694 ± 0.024	12.843 ± 0.042	Vega mag
2MASS H	9.437 ± 0.023	10.788 ± 0.025	11.990 ± 0.039	Vega mag
2MASS K_s	9.139 ± 0.021	10.524 ± 0.025	11.774 ± 0.034	Vega mag
WISE W1	8.936 ± 0.023	10.381 ± 0.035	...	Vega mag
WISE W2	8.963 ± 0.020	10.450 ± 0.036	...	Vega mag
WISE W3	8.995 ± 0.041	10.134 ± 0.157	...	Vega mag
IRAC 3.6	8.915 ± 0.042	10.322 ± 0.028	11.647 ± 0.040	Vega mag
IRAC 4.5	8.887 ± 0.044	10.309 ± 0.029	11.619 ± 0.051	Vega mag
Isochrone-inferred Parameters				
Effective temperature T_{eff}	4360 ± 10	4760 ± 10	4900 ± 10	K
Surface gravity $\log g$	0.90 ± 0.01	0.84 ± 0.01	$1.72^{+0.03}_{-0.02}$	cm s $^{-2}$
Luminosity L_*	900^{+10}_{-20}	1570 ± 10	210 ± 10	L_\odot
Radius R_*	53 ± 1	62 ± 1	20 ± 1	R_\odot
Distance d_{iso}	5.6 ± 0.1	12.4 ± 0.1	$7.9^{+0.2}_{-0.3}$	kpc
Mass M_*	0.80 ± 0.01	0.98 ± 0.01	0.79 ± 0.01	M_\odot
Age τ	12.4 ± 0.1	10.0 ± 0.1	12.3 ± 0.5	Gyr
Extinction A_V	3.10 ± 0.02	3.25 ± 0.01	2.71 ± 0.03	mag

Table 2 continued

Table 2 (continued)

Property	J172452.74-281459.4	J175228.08-320947.6	J175836.79-313707.6	Units
Spectroscopy-inferred Properties and Parameters				
Radial velocity v_r	$+9.23 \pm 1$	-63.98 ± 1	-196.42 ± 1	km s^{-1}
Microturbulence ξ	$2.78^{+0.03}_{-0.01}$	$3.22^{+0.05}_{-0.04}$	2.69 ± 0.04	km s^{-1}
Metallicity [Fe/H]	-2.03 ± 0.18	-2.56 ± 0.22	-3.15 ± 0.25	
Non-LTE corrected metallicity [Fe/H] _{NLTE}	-1.95	-2.44	-3.06	
Galactic Orbit Parameters				
Total Galactic velocity v	89 ± 3	102 ± 4	220 ± 3	km s^{-1}
Pericenter of Galactic orbit R_{peri}	0.3 ± 0.1	0.8 ± 0.1	0.1 ± 0.1	kpc
Apocenter of Galactic orbit R_{apo}	2.7 ± 0.1	4.5 ± 0.1	$1.5^{+0.2}_{-0.1}$	kpc
Eccentricity of Galactic orbit e	$0.77^{+0.03}_{-0.04}$	$0.70^{+0.02}_{-0.03}$	$0.84^{+0.03}_{-0.07}$	
Maximum distance from Galactic plane z_{max}	$1.18^{+0.05}_{-0.04}$	$0.77^{+0.03}_{-0.04}$	0.92 ± 0.05	kpc

In parallel we obtained spectroscopic stellar parameter using the classical excitation/ionization balance approach. We measured the equivalent widths of Fe I and Fe II atomic absorption lines in our continuum-normalized spectra by fitting Gaussian profiles with the `splot` task in `IRAF`. We used the `deblend` task to disentangle absorption lines from adjacent spectral features whenever necessary. The atomic data for Fe I and Fe II are from `linemake` (Sneden et al. 2009, 2016) maintained by Vinicius Placco and Ian Roederer⁹ as collected in Ji et al. (2020, submitted). We report our input atomic data, measured equivalent widths, and inferred abundances in Table 3.

We used 1D plane-parallel α -enhanced ATLAS9 model atmospheres (Castelli & Kurucz 2004), the 2019 version of the `MOOG` radiative transfer code (Sneden 1973), and the `q2 MOOG` wrapper¹⁰ (Ramírez et al. 2014) to calculate T_{eff} , $\log g$, $[\text{Fe}/\text{H}]$, and microturbulence ξ by simultaneously minimizing:

1. the difference between our inferred Fe I and Fe II abundances;
2. the dependence of Fe I abundance on excitation potential;
3. the dependence of Fe I abundance on reduced equivalent width.

We initiated our optimization with reasonable guesses for $[\text{Fe}/\text{H}]$ and ξ plus T_{eff} and $\log g$ 500 K and 1.0 dex lower than the isochrone-inferred parameters. We find the spectroscopic stellar parameters listed in Table 4. Due to the low S/N of our spectra blueward of 600 nm, we only analyzed Fe I and Fe II lines with $\lambda \geq 500$ nm. As a result, we cannot reliably measure a large number of Fe I lines over a wide range of excitation potential. In addition, most unblended Fe II lines in the spectra of metal-poor giants have $\lambda < 500$ nm. These two issues make it difficult to infer stellar parameters in a robust way using spectroscopy alone.

It has long been known that spectroscopic stellar parameters inferred for metal-poor giants using the classical approach differ from those derived using photometry and parallax information (e.g., Korn et al. 2003; Frebel et al. 2013; Mucciarelli & Bonifacio 2020). Since local thermodynamic equilibrium (LTE) is almost always assumed in the model atmospheres used to interpret equivalent width measurements, these differences are often attributed to the violation of the assumptions of LTE in

the photospheres of metal-poor giants. As a result, we impose the constraints on T_{eff} and $\log g$ deduced from our isochrone analysis and use the same optimization strategy to search for a self-consistent set of spectroscopic stellar parameters T_{eff} , $\log g$, $[\text{Fe}/\text{H}]$, and ξ using the classical excitation/ionization balance approach.

We calculated our adopted $[\text{Fe}/\text{H}]$ and ξ uncertainties due to our uncertain T_{eff} and $\log g$ estimates using a Monte Carlo simulation. On each iteration, we randomly sample self-consistent pairs of T_{eff} and $\log g$ from our isochrone posteriors and calculate the best $[\text{Fe}/\text{H}]$ and ξ using the classical excitation/ionization balance approach. After we find a converged solution, we calculate mean iron abundances using our Fe I and Fe II equivalent width measurements assuming the stellar parameters found on that iteration. We save the result of each iteration and calculate $[\text{Fe}/\text{H}]$ and its uncertainty as the (16,50,84) percentiles of the resulting metallicity distribution ($[\text{Fe}/\text{H}] = -2.03_{-0.01}^{+0.01}$ for 2MASS J172452.74-281459.4, $[\text{Fe}/\text{H}] = -2.58_{-0.01}^{+0.01}$ for 2MASS J175228.08-320947.6, and $[\text{Fe}/\text{H}] = -3.15_{-0.01}^{+0.02}$ for 2MASS J175836.79-313707.6). We then take these uncertainties and the converged stellar parameters described in the preceding paragraph and use them to redo the isochrone calculation using the converged stellar parameters and their uncertainties in the likelihood calculation. We repeat this entire process three times to obtain our final stellar parameters presented in Table 2. The final uncertainties in Table 2 are larger than those described above because the values in Table 2 account for both the standard deviation in iron abundance inferred from individual lines and the uncertainties due to our imperfectly estimated stellar parameters derived from the Monte Carlo analysis. The precise T_{eff} and $\log g$ resulting from our isochrone analysis imply that the ultimate accuracy of our $[\text{Fe}/\text{H}]$ estimate is limited by the uncertainties in our measured equivalent widths. As a final check, we used our measured Fe I and Fe II equivalent widths and initiated our optimization process using the final set of stellar parameters listed in Table 2. We find that the spectroscopically inferred stellar parameters that result are consistent within their uncertainties to our preferred values in Table 2.

In addition, we used the Casagrande et al. (2010) Infrared Flux Method (IRFM) to verify our isochrone-inferred T_{eff} . We deredden the 2MASS $J - K_s$ colors of our stars using the bulge-specific reddening maps from Gonzalez et al. (2011, 2012). In the IRFM calculation itself, we used the adopted $\log g$ and $[\text{Fe}/\text{H}]$ given in Table 2. For 2MASS J172452.74-281459.4, 2MASS J175228.08-320947.6, and 2MASS J175836.79-313707.6 we find IRFM $T_{\text{eff}} \approx 4530 \pm 350$ K, 4780 \pm

⁹ <https://github.com/vmplacco/linemake>

¹⁰ <https://github.com/astroChasqui/q2>

Table 3. Line List, Equivalent-width Measurements, and Abundances

Star	Wavelength (Å)	Species	Excitation Potential (eV)	log gf	Equivalent Width (mÅ)	ϵ_x
J172452.74-281459.4	5682.633	Na I	2.102	-0.706	20.70	4.330
J172452.74-281459.4	5688.203	Na I	2.104	-0.406	36.50	4.339
J172452.74-281459.4	5889.951	Na I	0.000	0.108	344.00	4.327
J175228.08-320947.6	5682.633	Na I	2.102	-0.706	3.00	3.728
J175228.08-320947.6	5688.203	Na I	2.104	-0.406	2.50	3.349
J175836.79-313707.6	5889.951	Na I	0.000	0.108	141.00	3.144
J172452.74-281459.4	5528.405	Mg I	4.346	-0.498	124.00	5.523
J172452.74-281459.4	5711.088	Mg I	4.343	-1.724	51.20	5.845
J175228.08-320947.6	5172.684	Mg I	2.712	-0.393	245.40	5.418
J175228.08-320947.6	5183.604	Mg I	2.717	-0.167	213.00	4.821
J175228.08-320947.6	5528.405	Mg I	4.346	-0.498	132.80	5.902
J175228.08-320947.6	5711.088	Mg I	4.343	-1.724	16.20	5.520
J175836.79-313707.6	5172.684	Mg I	2.712	-0.393	160.60	4.560
J175836.79-313707.6	5183.604	Mg I	2.717	-0.167	181.70	4.621

NOTE—This table is published in its entirety in the machine-readable format. A portion is shown here for guidance regarding its form and content.

Table 4. Spectroscopic Stellar Parameters

Star	T_{eff} (K)	log g	[Fe/H]	ξ (km s ⁻¹)
J172452.74-281459.4	4780 ± 240	1.40 ± 0.60	-1.90 ± 0.20	3.2 ± 0.7
J175228.08-320947.6	4790 ± 210	0.47 ± 0.51	-2.57 ± 0.20	3.4 ± 0.9
J175836.79-313707.6	4820 ± 280	1.94 ± 0.86	-3.27 ± 0.33	2.5 ± 0.5

400 K, and 4680 ± 400 K in accord with the isochrone-inferred T_{eff} for each star. The large uncertainties in the IRFM T_{eff} are due to the reddening uncertainties in the Gonzalez et al. (2011, 2012) map.

Finally, we calculated 1D non-LTE corrections to our individual iron line abundances using the Amarsi et al. (2016) grid. While that grid was calculated with MARCS model atmospheres (Gustafsson et al. 2008) and our iron abundances were calculated with ATLAS9 model atmospheres, both model atmospheres are very similar and we expect any differences to have only a small effect on our abundance corrections. We find that the mean non-LTE corrections for Fe I lines in our three giant stars to be 0.18, 0.18, and 0.14 dex for 2MASS J172452.74-281459.4, 2MASS J175228.08-320947.6, and 2MASS J175836.79-313707.6. The corrections are smaller for Fe II: 0.03, 0.03, and 0.04

for 2MASS J172452.74-281459.4, 2MASS J175228.08-320947.6, and 2MASS J175836.79-313707.6. These corrections are of the magnitude expected for giant stars in this metallicity regime (e.g., HD 122563 from Amarsi et al. 2016). We give our non-LTE [Fe/H] values in Table 2.

3.2. Stellar Orbits

To confirm that these giants located in the bulge are indeed on tightly bound orbits, we calculated their Galactic orbits using `galpy`¹¹. We sampled 1,000 Monte Carlo realizations from the Gaia DR2 astrometric solutions for each star using the distance posterior that results from our isochrone analysis while taking full ac-

¹¹ <https://github.com/jobovy/galpy>

count of the covariances between position, parallax, and proper motion. We used the radial velocities derived from our high-resolution MIKE spectra and assumed no covariance between our measured radial velocity and the Gaia DR2 astrometric solution. We used each Monte Carlo realization as an initial condition for an orbit and integrated it forward 10 Gyr in a Milky Way-like potential. We adopted the `MWPotential2014` described by Bovy (2015). In that model, the bulge is parameterized as a power-law density profile that is exponentially cut-off at 1.9 kpc with a power-law exponent of -1.8 . The disk is represented by a Miyamoto–Nagai potential with a radial scale length of 3 kpc and a vertical scale height of 280 pc (Miyamoto & Nagai 1975). The halo is modeled as a Navarro–Frenk–White halo with a scale length of 16 kpc (Navarro et al. 1996). We set the solar distance to the Galactic center to $R_0 = 8.122$ kpc, the circular velocity at the Sun to $V_0 = 238$ km s $^{-1}$, the height of the Sun above the plane to $z_0 = 25$ pc, and the solar motion with the respect to the local standard of rest to $(U_\odot, V_\odot, W_\odot) = (10.0, 11.0, 7.0)$ km s $^{-1}$ (Juric et al. 2008; Bland-Hawthorn & Gerhard 2016; Gravity Collaboration et al. 2018). We give the resulting Galactic orbits in Table 2. We find that the Galactic orbits of all three giant stars have apocenters $R_{\text{apo}} \lesssim 4$ kpc, confirming that they are all indeed tightly bound to the Galaxy and confined to the bulge region.

4. CHEMICAL ABUNDANCES

We measured the equivalent widths of atomic absorption lines for Na I, Mg I, Al I, Si I, Ca I, Sc II, Ti I, Ti II,

Cr I, Cr II, Mn I, Co I, Ni I, Cu I, Zn I, Sr II, Y II, Ba II, and La II in our continuum-normalized spectra by fitting Gaussian profiles with the `splot` task in IRAF. We used the `deblend` task to disentangle absorption lines from adjacent spectral features whenever necessary. We measured an equivalent width for every transition in our line list that could be recognized as an absorption line regardless of S/N or wavelength, taking into consideration the quality of a spectrum in the vicinity of a line and the availability of alternative transitions of the same species. We employed the 1D plane-parallel α -enhanced ATLAS9 model atmospheres and the 2019 version of MOOG to calculate abundances for each equivalent width. In addition, we used spectral synthesis to infer the abundance of Eu II and to confirm the equivalent-width based abundance of Ba II. We report our input atomic data from Ji et al. (2020, submitted), measured equivalent widths, and individual inferred abundances in Table 3. We present our adopted mean chemical abundances and associated uncertainties in Table 5. The standard deviation of abundances inferred for individual lines σ_ϵ does not take into account the uncertainties in our adopted stellar parameters. The uncertainties in individual abundances relative to iron $\sigma_{[X/Fe]}$ include both the standard deviation of abundances inferred for individual lines and the spectroscopic stellar parameter uncertainties assuming local thermodynamic equilibrium. We plot these later uncertainties in Figures 3, 5, 6, and 8.

Table 5. Chemical Abundances

Star	Species	N	ϵ_X	σ_ϵ	[X/H]	[X/Fe]	$\sigma_{[X/Fe]}$
J172452.74-281459.4	Na I	3	4.332	0.003	-1.908	0.124	0.012
	Na INLTE	3	4.204	...	-2.036	-0.004	...
	Mg I	2	5.684	0.114	-1.916	0.116	0.161
	Al I	2	4.828	0.066	-1.622	0.410	0.093
	Si I	5	5.726	0.026	-1.784	0.248	0.029
	Ca I	18	4.607	0.081	-1.733	0.299	0.084
	Sc II	5	1.250	0.073	-1.900	0.132	0.082
	Ti I	42	3.157	0.062	-1.884	0.148	0.065
	Ti II	50	2.922	0.126	-2.028	0.004	0.127
	$\overline{\text{Ti}}$...	3.029	...	-1.921	0.111	0.106
	Cr I	7	3.254	0.148	-2.386	-0.354	0.161
	Cr II	2	4.027	0.237	-1.613	0.419	0.336
	Mn I	3	2.796	0.014	-2.634	-0.602	0.020
	Fe I	22	5.309	0.174	-2.191
	Fe II	12	5.626	0.182	-1.874
	Co I	5	3.146	0.044	-1.844	0.188	0.050
Ni I	14	4.256	0.056	-1.964	0.068	0.059	

Table 5 continued

Table 5 (continued)

Star	Species	N	ϵ_X	σ_ϵ	[X/H]	[X/Fe]	$\sigma_{[X/Fe]}$
	Zn I	2	2.958	0.117	-1.602	0.430	0.166
	Sr I	1	1.124	0.000	-1.746	0.286	0.016
	Sr II	2	≥ -1.280	...	≥ -4.150	≥ -2.118	...
	Y II	3	-0.076	0.027	-2.286	-0.254	0.034
	Ba II	2	0.131	0.080	-2.049	-0.017	0.113
	La II	2	≤ -0.154	...	≤ -1.254	≤ 0.778	...
J175228.08-320947.6	Na I	2	3.538	0.134	-2.702	-0.144	0.190
	Na I _{NLTE}	2	3.445	...	-2.795	-0.236	...
	Mg I	4	5.415	0.194	-2.185	0.373	0.225
	Al I	1	3.889	0.000	-2.561	-0.003	0.032
	Si I	5	5.646	0.061	-1.864	0.694	0.069
	Ca I	15	4.053	0.071	-2.287	0.271	0.073
	Sc II	5	0.665	0.090	-2.485	0.073	0.101
	Ti I	28	3.156	0.119	-1.885	0.673	0.121
	Ti II	36	2.414	0.088	-2.536	0.022	0.089
	Ti	...	2.739	...	-2.211	0.347	0.102
	Cr I	5	3.037	0.190	-2.603	-0.045	0.212
	Cr II	4	2.822	0.109	-2.818	-0.260	0.126
	Mn I	3	2.817	0.138	-2.613	-0.055	0.169
	Fe I	50	4.871	0.218	-2.629
	Fe II	6	5.055	0.223	-2.445
	Co I	4	3.199	0.041	-1.791	0.767	0.048
	Ni I	9	3.911	0.074	-2.309	0.249	0.079
	Zn I	1	2.251	0.000	-2.309	0.249	0.003
	Sr I	1	0.898	0.000	-1.972	0.586	0.007
	Sr II	1	0.076	0.000	-2.794	-0.236	0.040
	Y II	2	-0.392	0.061	-2.602	-0.044	0.087
	Ba II	2	-1.262	0.077	-3.442	-0.884	0.109
	La II	2	≤ -0.318	...	≤ -1.418	≤ 1.140	...
J175836.79-313707.6	Na I	1	3.144	0.000	-3.096	0.050	0.025
	Na I _{NLTE}	1	2.778	...	-3.462	-0.312	...
	Mg I	2	4.591	0.022	-3.009	0.137	0.041
	Al I	1	≤ 3.064	...	≤ -3.386	≤ -0.240	...
	Si I	4	5.050	0.224	-2.460	0.686	0.259
	Ca I	15	3.529	0.088	-2.811	0.335	0.092
	Sc II	3	0.390	0.032	-2.760	0.386	0.042
	Ti I	27	3.293	0.115	-1.748	1.398	0.119
	Ti II	42	2.489	0.133	-2.461	0.685	0.135
	Ti	...	2.804	...	-2.146	1.000	0.131
	Cr I	4	2.598	0.014	-3.042	0.104	0.025
	Cr II	3	2.926	0.231	-2.714	0.432	0.283
	Mn I	3	2.769	0.067	-2.661	0.485	0.083
	Fe I	42	4.325	0.244	-3.175
	Fe II	6	4.161	0.264	-3.339
	Co I	1	2.561	0.000	-2.429	0.717	0.020
	Ni I	6	3.442	0.123	-2.778	0.368	0.136
	Cu I	1	1.817	0.000	-2.373	0.773	0.020
	Zn I	2	2.209	0.016	-2.351	0.795	0.024
	Sr II	2	-0.950	0.058	-3.820	-0.674	0.086
	Y II	3	-0.289	0.111	-2.499	0.647	0.136
	Ba II	3	-1.293	0.165	-3.473	-0.327	0.202
	La II	1	≤ -0.286	...	≤ -1.386	≤ 1.760	...

NOTE—Abundance ratios assume [Asplund et al. \(2009\)](#) solar photospheric abundances.

To serve as comparison samples, we collected chemical abundances for outer bulge stars and halo stars from the

literature. Our outer bulge comparison sample comes from [García Pérez et al. \(2013\)](#), [Casey & Schlafman](#)

(2015), Howes et al. (2015, 2016), Lamb et al. (2017), and Lucey et al. (2019). Our halo comparison sample comes from Cayrel et al. (2004), Bonifacio et al. (2009a), and Reggiani et al. (2017). We note that the current sample of metal-poor bulge stars shows larger abundance dispersions than the sample of well-studied halo stars for all elements. These large dispersions are most likely due to the lower S/N of the input bulge spectra combined with the lack of a large-scale homogeneous abundance analyses in the metal-poor bulge. On the other hand, it could also be that the metal-poor stars in the bulge are first-generation Population II (Pop II) stars for which the large dispersions appear because each star records the nucleosynthesis of individual Population III (Pop III) supernovae. While we regard the former as more likely, only a large-scale homogeneous abundance analysis of hundreds of metal-poor bulge stars will settle the issue.

4.1. α Elements

Oxygen, magnesium, silicon, calcium, and titanium are often referred to as α elements. Magnesium, silicon, and calcium are formed via similar nucleosynthetic channels. Magnesium is mainly formed via carbon burning in core-collapse supernovae (thermonuclear supernovae provide an order of magnitude less). Silicon is mostly a product of oxygen burning and is itself the most abundant product of oxygen burning. Core-collapse and thermonuclear supernovae contribute to silicon production in equal proportion. Calcium is the product of both hydrostatic and explosive oxygen and silicon burning. It is mostly produced in core-collapse supernovae. Even though titanium forms either in the α -rich freeze-out of shock-decomposed nuclei during core-collapse supernovae or in explosive ^4He fusion in the envelopes of CO white dwarfs during thermonuclear supernovae (e.g., Woosley & Weaver 1994; Livne & Arnett 1995), it is often considered alongside the true α elements because of their correlated chemical abundances (Clayton 2003).

We plot in Figure 3 our inferred α abundances. We find that our metal-poor giants in the inner bulge roughly track the α abundances observed in the outer bulge and halo comparison samples. The one exception is the high Ti I and Ti II abundances we infer for our most metal-poor star 2MASS J175836.79-313707.6. We plot in Figure 4 a representative Ti II line of 2MASS J175836.79-313707.6 in comparison to the same line observed in BPS CS 30312-0059, a star from Roederer et al. (2014) with very similar spectroscopic stellar parameters ($T_{\text{eff}} = 4780$ K, $\log g = 1.4$, and $[\text{Fe}/\text{H}] = -3.3$). We will argue in Section 5 that the high titanium abundance in 2MASS J175836.79-313707.6 is best explained by ex-

plosive ^4He fusion in the envelope of a CO white dwarf accreting from a helium star binary companion during a Chandrasekhar-mass thermonuclear supernova.

The silicon abundances we infer from individual transitions for our three inner bulge giants have non-negligible scatter and are affected by our stellar parameter uncertainties. Nevertheless, our inferred abundances are in accord with silicon abundance inferences in outer bulge giants with $[\text{Fe}/\text{H}] \approx -3.2$ and follow the same trend observed at higher metallicities. We observe the largest silicon abundances in our most metal-poor inner bulge giant 2MASS J175836.79-313707.6. Most of the accessible silicon lines redward of 500 nm are weak in such a metal-poor giant, so we also measured two additional lines at 3906 and 4103 Å that were identifiable in its spectrum even at $S/N \approx 5/\text{pixel}$ at 400 nm. The apparent difference between the silicon abundances inferred for halo dwarfs and giants is usually attributed to non-LTE effects even though other factors play a role (e.g., Bonifacio et al. 2009b, Amarsi et al. 2020, submitted). According to the Amarsi & Asplund (2017) grid of non-LTE corrections¹², the typical non-LTE silicon abundance correction for a giant star with parameters similar to 2MASS J175836.79-313707.6 (i.e., $T_{\text{eff}} = 4500$ K, $\log g = 1.5$, $[\text{Fe}/\text{H}] = -3.0$, $\xi = 2$ km s⁻¹, and $\epsilon_{\text{Si}} \approx 5.01$) is about -0.02 dex. Non-LTE corrections are more important for metal-poor dwarfs, as a dwarf with a similar metallicity ($T_{\text{eff}} = 6500$ K, $\log g = 4.5$, $[\text{Fe}/\text{H}] = -3.0$, $\xi = 1$ km s⁻¹, and $\epsilon_{\text{Si}} \approx 5.01$) will have a non-LTE silicon correction of about $+0.25$ dex.

4.2. Light Odd-Z Elements

Like magnesium, sodium is mostly produced in core-collapse supernovae via carbon burning. Unlike magnesium, the surviving fraction of sodium in supernovae ejecta depends on metallicity so it is treated as a secondary product. Sodium is also produced as a product of hydrogen and helium fusion in thermonuclear explosions, though in smaller quantities than in core-collapse supernovae. Similar to sodium, aluminum is synthesized during carbon fusion in core-collapse supernovae in a secondary reaction that is dependent on the amount of ^{22}Ne burned (which in turn depends on the carbon and oxygen content of the star). In contrast to sodium and aluminum, scandium is formed via both oxygen burning in core-collapse supernovae and as a product of α -rich freeze-out in the shocked region just above the rebounded core (the same region responsible for ^{44}Ti e.g., Clayton 2003).

¹² <http://www.mpia.de/homes/amarsi/index.html>

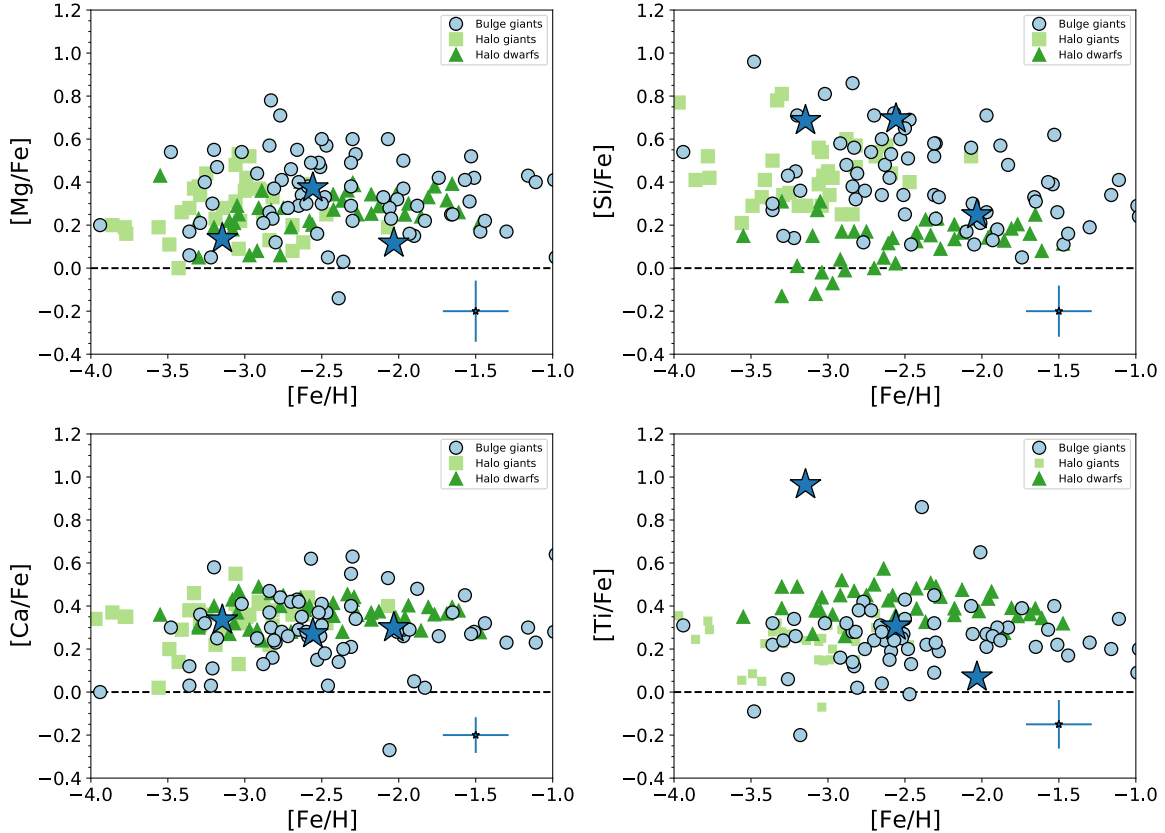


Figure 3. Abundances of α elements magnesium, silicon, calcium, and titanium relative to iron. We plot as blue stars our three metal-poor inner bulge giants. We plot as light blue circles a literature compilation of metal-poor outer bulge stars from [García Pérez et al. \(2013\)](#), [Casey & Schlafman \(2015\)](#), [Howes et al. \(2015, 2016\)](#), [Lamb et al. \(2017\)](#), and [Lucey et al. \(2019\)](#). We plot as light green squares halo giants from [Cayrel et al. \(2004\)](#) and as dark green triangles halo dwarfs from [Bonifacio et al. \(2009a\)](#) & [Reggiani et al. \(2017\)](#). The point with error bars in the bottom right of each panel corresponds to the mean uncertainty of our three stars. We find that the α -element abundances of the inner and outer bulge are consistent with those in the halo. The high $[\text{Si}/\text{Fe}] \approx +0.7$ abundance in our most metal-poor star 2MASS J175836.79-313707.6 is suggestive of nucleosynthesis in an oxygen-rich environment while the $[\text{Ti}/\text{Fe}] \approx +1.0$ abundance could be the result of a Chandrasekhar-mass thermonuclear supernova of a CO white dwarf accreting from a helium star companion.

We plot in Figure 5 our inferred light odd- Z abundances. We find that our metal-poor giants in the inner bulge roughly track the light odd- Z abundances observed in the outer bulge and halo comparison samples. The one exception is the high scandium abundance we infer for our most metal-poor star 2MASS J175836.79-313707.6. We will argue in Section 5 that the high scandium abundance in 2MASS J175836.79-313707.6 is produced by nucleosynthesis in oxygen-rich extreme Pop II stars.

Sodium abundance inferences are strongly affected by departures from LTE, as the main sodium abundance indicator in our spectra is the resonant sodium doublet at 5889/5895 Å. We corrected our abundances inferred under the assumptions of LTE using the [Lind et al. \(2011\)](#)

correction grid provided via the INSPECT project¹³. To correct the abundances of 2MASS J172452.74-281459.4 and 2MASS J175228.08-320947.6, we used the correction for a star with $\log g = 1$ as our adopted gravities were outside the bounds of the available grid. The sodium doublet is affected by interstellar medium (ISM) absorption, and the extreme extinction along the line of sight to the inner bulge can affect both the shape and depth of the sodium doublet. As a result, we were unable to disentangle the effects of photospheric and ISM absorption for the 5895 Å line and we do not use it in our analysis. Two weaker sodium lines at 5682 and 5688 Å are available in the spectra of 2MASS J172452.74-281459.4 and 2MASS J175228.08-320947.6 though, and all abundances inferred from measured lines are in good

¹³ <http://inspect.coolstars19.com/>

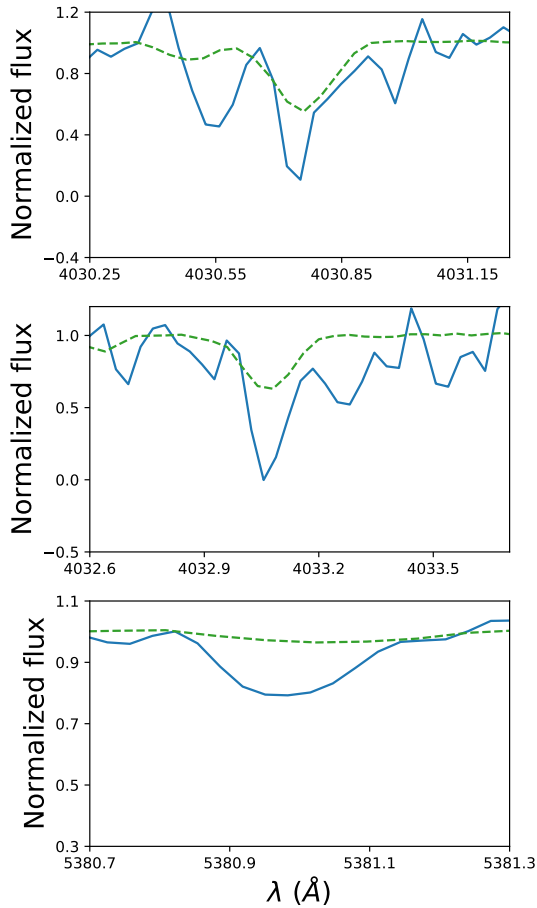


Figure 4. Comparison of manganese and titanium lines for 2MASS J175836.79-313707.6 and BPS CS 30312-0059, a star from [Roederer et al. \(2014\)](#) with very similar spectroscopic stellar parameters ($T_{\text{eff}} = 4780$ K, $\log g = 1.4$, and $[\text{Fe}/\text{H}] = -3.3$). Top and middle: comparison of two Mn I lines for 2MASS J175836.79-313707.6 (solid blue line) and BPS CS 30312-0059 (dashed green line) Bottom: comparison of a Ti II line for 2MASS J175836.79-313707.6 (solid blue line) and BPS CS 30312-0059 (dashed green line).

agreement. For 2MASS J175836.79-313707.6, we only have the 5889 Å line. Its spectrum has good S/N and is clear of ISM absorption, so we believe our inferred sodium abundance is reliable. Most of the sodium abundances in our comparison outer bulge and halo samples have been corrected for departures from local thermodynamic equilibrium. [Cayrel et al. \(2004\)](#) used corrections from [Baumueller et al. \(1998\)](#) while [Bonifacio et al. \(2009a\)](#) used corrections from [Andrievsky et al. \(2007\)](#). Like our sodium abundances, [Howes et al. \(2015, 2016\)](#) and [Reggiani et al. \(2017\)](#) were non-LTE corrected using the grid from [Lind et al. \(2011\)](#). [Casey & Schlafman \(2015\)](#) and [Lucey et al. \(2019\)](#) did not account for non-LTE effects.

It was extremely difficult to infer aluminum abundances for our three stars. The best available aluminum lines in metal-poor stars are usually the 3944 and 3961 Å lines, and the spectra of our highly extinguished inner bulge stars have very low S/N at $\lambda < 400$ nm. We were unable to measure the equivalent width of either line in 2MASS J172452.74-281459.4. We were only able to measure upper limits for the equivalent widths of the 3944 Å line in 2MASS J175836.79-313707.6 and the 3961 Å line in 2MASS J175228.08-320947.6. While there are two weaker aluminum lines at 6696 and 6698 Å, they were only able to provide an upper limit on the aluminum abundance of 2MASS J172452.74-281459.4. While we report aluminum abundances assuming LTE in Table 5, to fairly compare our aluminum abundances with the outer bulge and halo samples we follow [Reggiani et al. \(2017\)](#) and add 0.65 dex to the LTE abundances of our three stars as well as the LTE abundances in the comparison samples.

We inferred the scandium abundances of our three inner bulge giants using Sc II lines accounting for hyperfine structure (HFS) using data taken from the Kurucz compilation¹⁴. Similar to what we observed with titanium, the abundance of scandium in 2MASS J175836.79-313707.6 is enhanced relative to the comparison samples.

4.3. Iron-peak Elements

Iron-peak elements can be formed directly or as a byproduct of explosive silicon burning, either incomplete (chromium and manganese) or complete (cobalt, nickel, and zinc). Their nucleosynthesis mainly takes place in thermonuclear supernovae (e.g., [Clayton 2003](#); [Grimmett et al. 2019](#)). The observed increase in the abundance ratios $[\text{Co}/\text{Fe}]$ and $[\text{Zn}/\text{Fe}]$ with decreasing $[\text{Fe}/\text{H}]$ in metal-poor stars combined with the dependence of cobalt and zinc yields on the explosion energies of core-collapse supernovae also point to contributions from hypernovae events at $[\text{Fe}/\text{H}] \lesssim -3.0$ (e.g., [Cayrel et al. 2004](#); [Reggiani et al. 2017](#)).

We plot in Figure 6 our inferred iron-peak abundances. We find that our metal-poor giants in the inner bulge consistently have higher iron-peak abundances than the outer bulge and halo comparison samples. We also find a significantly supersolar manganese abundance $[\text{Mn}/\text{Fe}] \approx +0.5$ for our most metal-poor star 2MASS J175836.79-313707.6. We do not correct our inferred iron-peak abundances for non-LTE effects, both because correction grids are lacking for all iron-

¹⁴ <http://kurucz.harvard.edu/linelists.html>

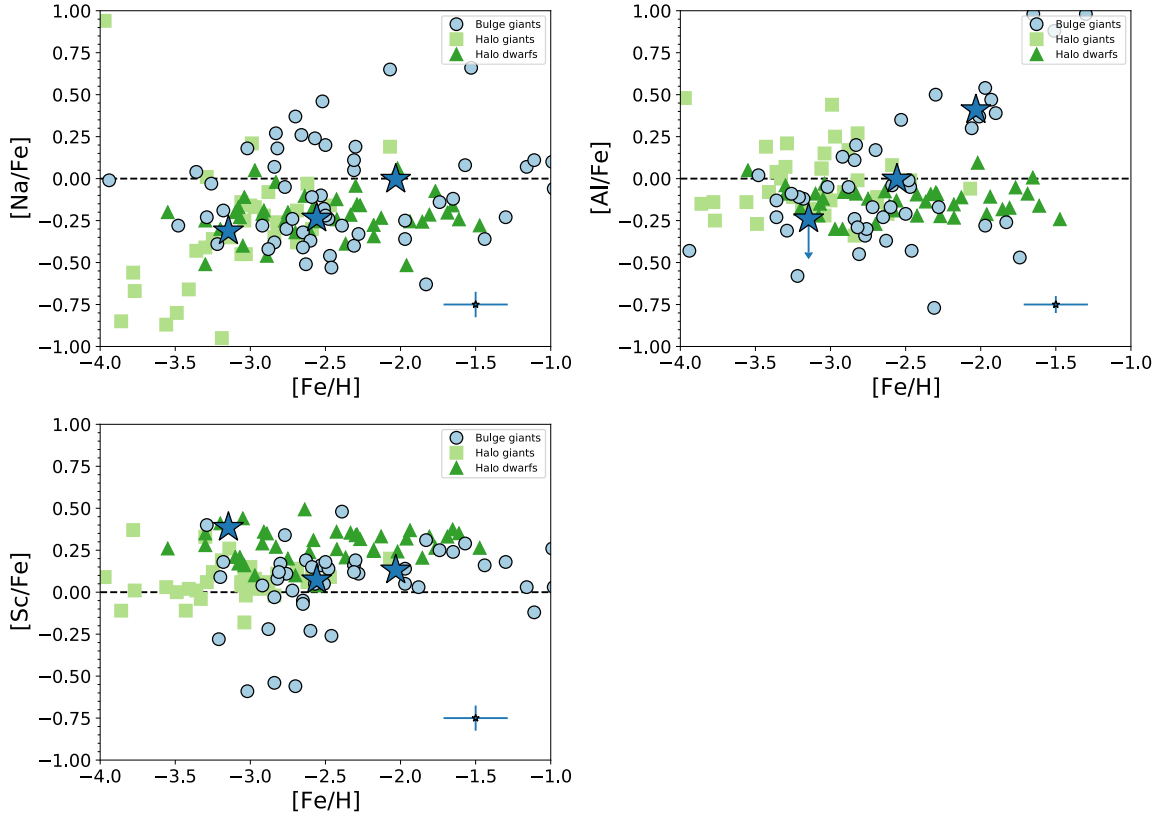


Figure 5. Abundances of light odd- Z elements sodium, aluminum, and scandium relative to iron. We plot as blue stars our three metal-poor inner bulge giants. We plot as light blue circles a literature compilation of metal-poor outer bulge stars from García Pérez et al. (2013), Casey & Schlafman (2015), Howes et al. (2015, 2016), Lamb et al. (2017), and Lucey et al. (2019). We plot as light green squares halo giants from Cayrel et al. (2004) and as dark green triangles halo dwarfs from Bonifacio et al. (2009a) & Reggiani et al. (2017). The point with error bars in the bottom right of each panel corresponds to the mean uncertainty of our three stars. We find that the light odd- Z element abundances of the inner and outer bulge are consistent with those in the halo. The high $[\text{Sc}/\text{Fe}] \approx +0.4$ in our most metal-poor star 2MASS J175836.79-313707.6 is suggestive of nucleosynthesis in an oxygen-rich environment.

peak elements and because the iron-peak abundances in our comparison samples have not been corrected for departures from the assumptions of LTE. We will argue in Section 5 that the supersolar manganese abundance in 2MASS J175836.79-313707.6—and indeed its entire iron-peak abundance pattern—is best explained by nucleosynthesis in a thermonuclear supernova.

We plot Cr I abundances in Figure 6 despite the fact that those lines are strongly affected by departures from LTE (e.g., Bergemann & Cescutti 2010; Reggiani et al. 2017). We prefer Cr I to Cr II in this case because our inferred $[\text{Cr II}/\text{Fe}]$ ratio in Table 5 is significantly supersolar for 2MASS J175836.79-313707.6. Chromium almost always appears in solar $[\text{Cr}/\text{Fe}]$ ratios and neither core-collapse or thermonuclear supernovae produce $[\text{Cr}/\text{Fe}] \gtrsim +0.3$ (e.g., Clayton 2003; Grimmett et al. 2019). We therefore suspect that our inferred Cr II abundances are affected by noise in our spectra.

We find relatively high $[\text{Mn}/\text{Fe}]$ abundances in our inner bulge sample, including a significantly supersolar $[\text{Mn}/\text{Fe}] \approx +0.5$ in our most metal-poor star 2MASS J175836.79-313707.6. We plot in Figure 4 three Mn I lines for 2MASS J175836.79-313707.6 in comparison to the same lines observed in the comparison star BPS CS 30312-0059. We included HFS components in our abundance inferences using data taken from the Kurucz compilation referenced above but did not correct for departures from LTE. Corrections for departures from the assumptions of LTE in metal-poor giants tend to increase $[\text{Mn}/\text{Fe}]$ and would not change our conclusion about 2MASS J175836.79-313707.6 (e.g., Bergemann et al. 2019; Eitner et al. 2020). The manganese abundance in 2MASS J175836.79-313707.6 is based on three weak manganese lines at 6013, 6016, and 6021 Å. Our spectrum of 2MASS J175836.79-313707.6 has $S/N \gtrsim 50/\text{pixel}$ at 600 nm and even though they are at the limit of detectability, these three manganese lines all

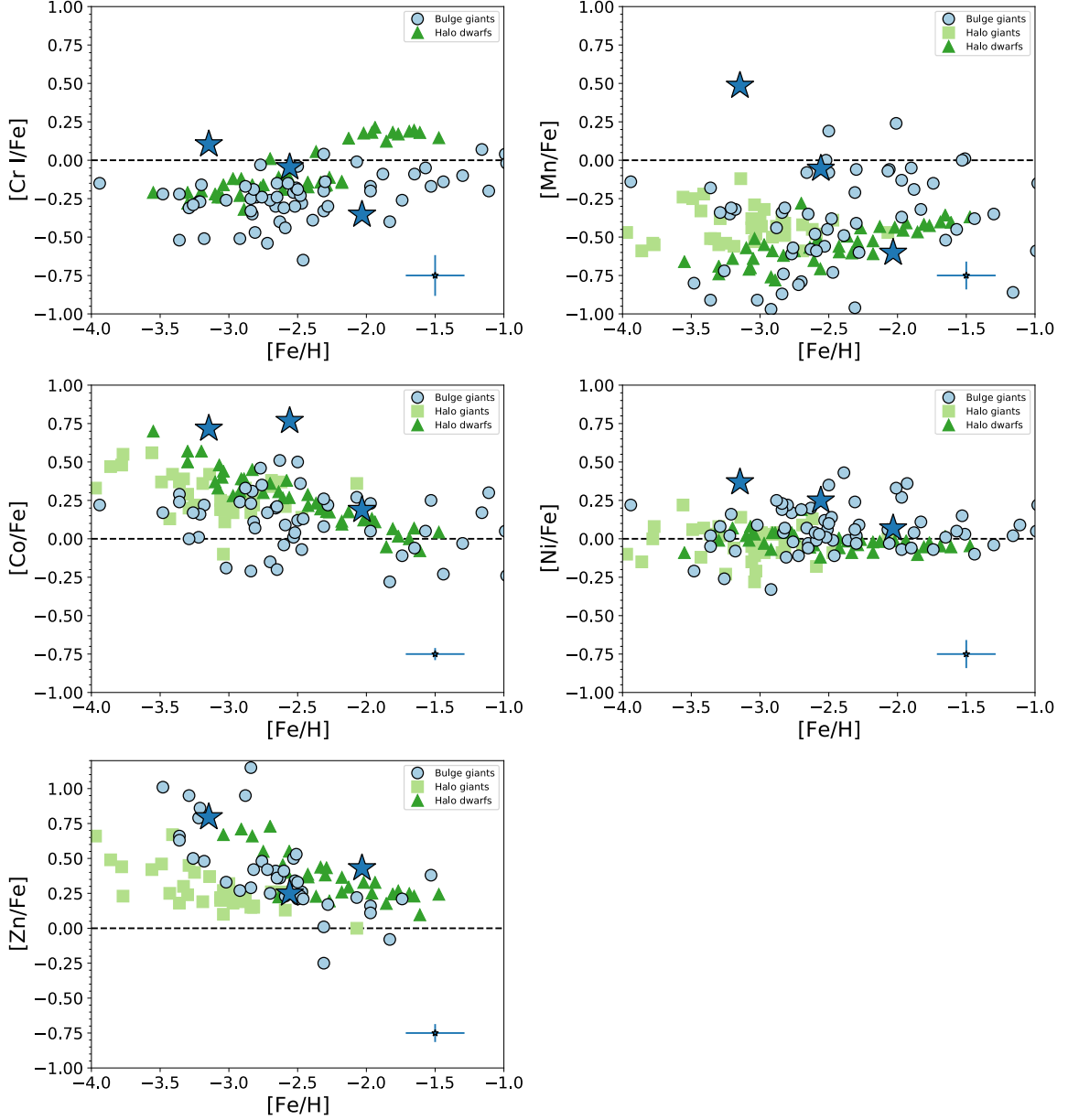


Figure 6. Abundances of iron-peak elements chromium, manganese, cobalt, nickel, and zinc. We plot as blue stars our three metal-poor inner bulge giants. We plot as light blue circles a literature compilation of metal-poor outer bulge stars from [García Pérez et al. \(2013\)](#), [Casey & Schlafman \(2015\)](#), [Howes et al. \(2015, 2016\)](#), [Lamb et al. \(2017\)](#), and [Lucey et al. \(2019\)](#). We plot as light green squares halo giants from [Cayrel et al. \(2004\)](#) and as dark green triangles halo dwarfs from [Bonifacio et al. \(2009a\)](#) & [Reggiani et al. \(2017\)](#). The point with error bars in the bottom right of each panel corresponds to the mean uncertainty of our three stars. For our three inner bulge stars, we find iron-peak abundances at the upper envelope of those observed in the outer bulge and halo. The significantly supersolar $[\text{Mn}/\text{Fe}]$ abundance ratio we find in our most metal-poor star 2MASS J175836.79-313707.6 is thought to be a clear sign of nucleosynthesis in a Chandrasekhar-mass thermonuclear supernova (e.g., [Seitenzahl et al. 2013a](#)).

appeared at their expected wavelengths and produce a consistent manganese abundance estimate. We therefore argue that the apparent lines are unlikely to be produced by noise in our spectrum. Although the bluer manganese lines typically analyzed in metal-poor giants are apparent in the spectrum of 2MASS J175836.79-313707.6, the abundances we infer from those lines are even higher.

We find relatively high cobalt abundances in our three metal-poor inner bulge giants, especially in the range $-2.5 \lesssim [\text{Fe}/\text{H}] \lesssim -2.0$. A comparison of cobalt lines observed in the spectra of 2MASS J175228.08-320947.6 and 2MASS J175836.79-313707.6 with lines synthesized assuming our adopted stellar parameters and cobalt abundances supports this finding (Figure 7). At the same time, our inferred zinc abundances closely track those observed in the outer bulge and halo dwarf samples. Our cobalt abundance estimates come from lines redward of 500 nm, while our zinc abundance estimates are based on lines blueward of 500 nm in the noisier parts of our spectra. We find supersolar nickel abundances in our three inner bulge stars. Like the outer bulge and halo comparison samples, we find no nickel abundance trend with metallicity. This lack of a dependence of nickel abundance on metallicity supports the idea that nickel can be used as a metallicity tracer in both the bulge and the halo (Singh et al. 2020).

4.4. Neutron-capture Elements

Elements beyond zinc are mostly produced by neutron-capture processes either “slow” or “rapid” relative to β decay timescales. The relative contributions of these s - and r -processes to the nucleosynthesis of each element are different and functions of metallicity. Some elements like strontium, yttrium, barium, and lanthanum are more commonly used as tracers of the s -process. On the other hand, europium is used as tracer of r -process nucleosynthesis (e.g., Cescutti et al. 2006; Jacobson & Friel 2013; Ji et al. 2016). Even though strontium and barium are usually used as tracers of the s -process, both can have important contributions from r -process nucleosynthesis at lower metallicities (e.g., Battistini & Bensby 2016; Casey & Schlafman 2017; Mashonkina & Belyaev 2019). Indeed, isotopic analyses of very metal-poor stars have shown that up to 80% of the barium in very metal-poor stars was synthesized in the r -process (Mashonkina & Belyaev 2019).

We plot in Figure 6 our inferred neutron-capture element abundances. We find that our metal-poor giants in the inner bulge roughly track the neutron-capture abundances observed in the outer bulge and halo comparison samples. For strontium, we used Sr II lines to infer its elemental abundances as those lines are not significantly

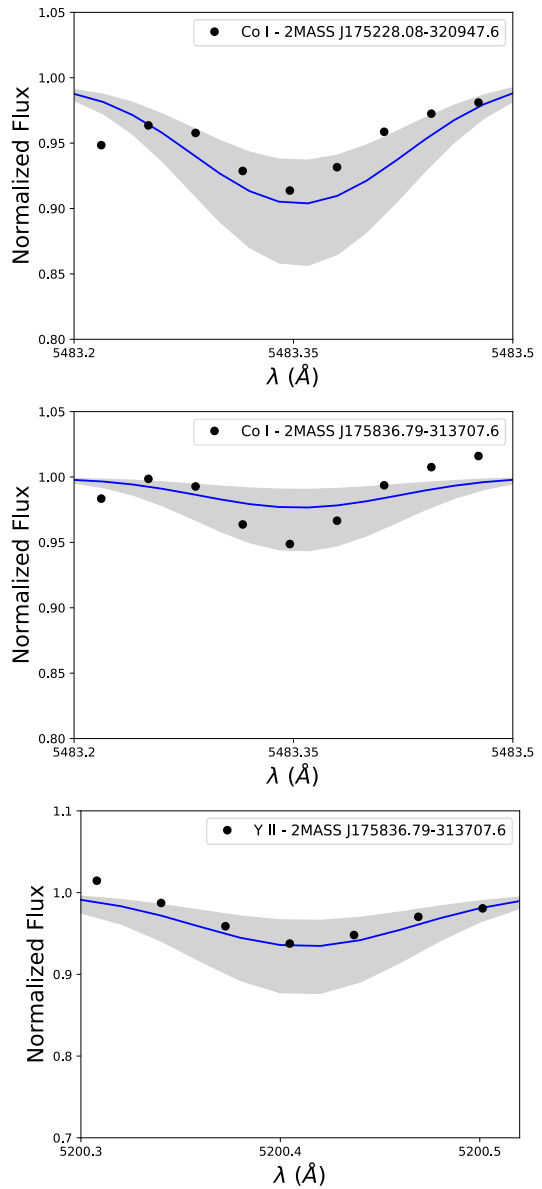


Figure 7. Comparison between observed and synthesized lines of cobalt and yttrium. In each panel we plot the observed flux in the vicinity of each line as black dots, the synthesized line assuming our adopted stellar parameters and abundances in blue, and the uncertainty in the synthesized line given our abundance uncertainties in gray. Top: a Co I line in the star 2MASS J175228.08-320947.6 compared with the line synthesized for cobalt abundance $A(\text{Co}) = 3.20 \pm 0.3$. Middle: the same Co I line in the star 2MASS J175836.79-313707.6 compared with the line synthesized for cobalt abundance $A(\text{Co}) = 2.56 \pm 0.3$. Bottom: a Y II line in the star 2MASS J175836.79-313707.6 compared with the line synthesized for yttrium abundance $A(\text{Y}) = -0.29 \pm 0.2$.

affected by departures from LTE (Hansen et al. 2013). For yttrium we used HFS components from the same Kurucz compilation referenced above, though we note that the S/N of our spectra in the vicinity of the yttrium lines were not high. Although we inferred our yttrium abundances using equivalent widths, the observed spectrum of 2MASS J175836.79-313707.6 is in good agreement with a synthesized Y II line at 5200 Å assuming our inferred abundance $A(Y) = -0.29 \pm 0.2$ (Figure 7). For barium, the abundances we infer using both equivalent widths and spectral synthesis based on unblended Ba II lines in parts of our spectra with high S/N agree within about 0.2 dex. For europium and lanthanum, the low S/N of the blue parts of our spectra only allow us to infer upper limits on their abundances.

5. DISCUSSION

The three metal-poor giants in the inner bulge we studied have orbits that are confined to the bulge. They are therefore likely to be among the oldest stars in the Milky Way and trace the earliest stage of the formation of the Milky Way’s oldest component: the bulge. We find that the abundances of our inner bulge stars at $[\text{Fe}/\text{H}] \gtrsim -3.0$ are for the most part in accord with the abundances of stars with similar metallicities in the outer bulge and halo.

The story is different for our most metal-poor inner bulge giant 2MASS J175836.79-313707.6 at $[\text{Fe}/\text{H}] = -3.15$. When compared to both the outer bulge and halo comparison samples, it has high $[\text{Ti}/\text{Fe}]$, $[\text{Sc}/\text{Fe}]$, and iron-peak abundances combined with supersolar $[\text{Mn}/\text{Fe}]$. We propose that 2MASS J175836.79-313707.6 is an ancient third-generation star with α and light odd- Z elements produced by massive Pop II stars that were seeded with abundant oxygen by massive Pop III stars. Unlike the progenitor(s) of the halo and the surviving dwarf galaxies, the intense star formation rate in the bulge will fully sample the stellar initial mass function and therefore produce many very massive stars. According to the Pop III supernovae yields of Heger & Woosley (2010), massive Pop III stars are prolific producers of oxygen relative to iron. After their supernovae, that overabundance of oxygen is transformed into an overabundance of scandium by the first generation of massive Pop II stars and injected into the interstellar medium by their supernovae. Titanium and the iron-peak elements including manganese in 2MASS J175836.79-313707.6 were simultaneously produced in the Chandrasekhar-mass thermonuclear supernova of a CO white dwarf accreting from a helium star binary companion. The combination of fast stellar evolution at low metallicities, relatively massive CO white dwarfs

produced by metal-poor stars, and efficient accretion from a helium star produced a short delay time comparable to the combined lifetimes of two generations of massive stars, about 10 Myr after the onset of star formation in what would become the bulge of the Milky Way.

To verify the scenario outlined above, we evaluate the ability of models predicting the nucleosynthetic yields of core-collapse and thermonuclear supernovae to reproduce the observed abundance pattern of 2MASS J175836.79-313707.6. Oxygen-rich metal-poor stars produce more scandium relative to iron than solar-composition metal-poor stars (e.g., Woosley & Weaver 1995; Chieffi & Limongi 2004). The Chandrasekhar-mass thermonuclear supernova of a CO white dwarf accreting from a helium star binary companion will produce large amounts of titanium and can explode with a short delay time (e.g., Woosley & Weaver 1994; Livne & Arnett 1995; Wang et al. 2009a,b). It is thought that near Chandrasekhar-mass thermonuclear supernovae are the only supernovae capable of producing $[\text{Mn}/\text{Fe}] \gtrsim 0$, as only CO white dwarfs near the Chandrasekhar mass have densities $\rho \gtrsim 2 \times 10^8 \text{ g cm}^{-3}$ necessary to produce large amounts of ^{55}Co that eventually decays into manganese (e.g., Seitzzahl et al. 2013a; Yamaguchi et al. 2015; Seitzzahl & Townsley 2017).

In an effort to confirm the scenario outlined above, we compare the abundances of 2MASS J175836.79-313707.6 with the yields predicted by three different classes of Chandrasekhar-mass thermonuclear supernovae plus one class of sub-Chandrasekhar-mass thermonuclear supernovae:

1. Chandrasekhar-mass deflagration to detonation transition (DDT) models with fixed C/O ratios from Seitzzahl et al. (2013b) and DDT models with variable C/O ratios from Ohlmann et al. (2014);
2. Chandrasekhar-mass pure (turbulent) deflagration models from Fink et al. (2014);
3. Chandrasekhar-mass gravitationally confined detonation (GCD) models from Seitzzahl et al. (2016);
4. sub-Chandrasekhar-mass models resulting from the merger of two $M_* = 0.6 M_\odot$ CO white dwarfs from Papish & Perets (2016).

We first fix the iron abundance predicted by each model to the metallicity of 2MASS J175836.79-313707.6 and select the model that minimizes χ^2 between our observed abundances and the predicted yields. If we

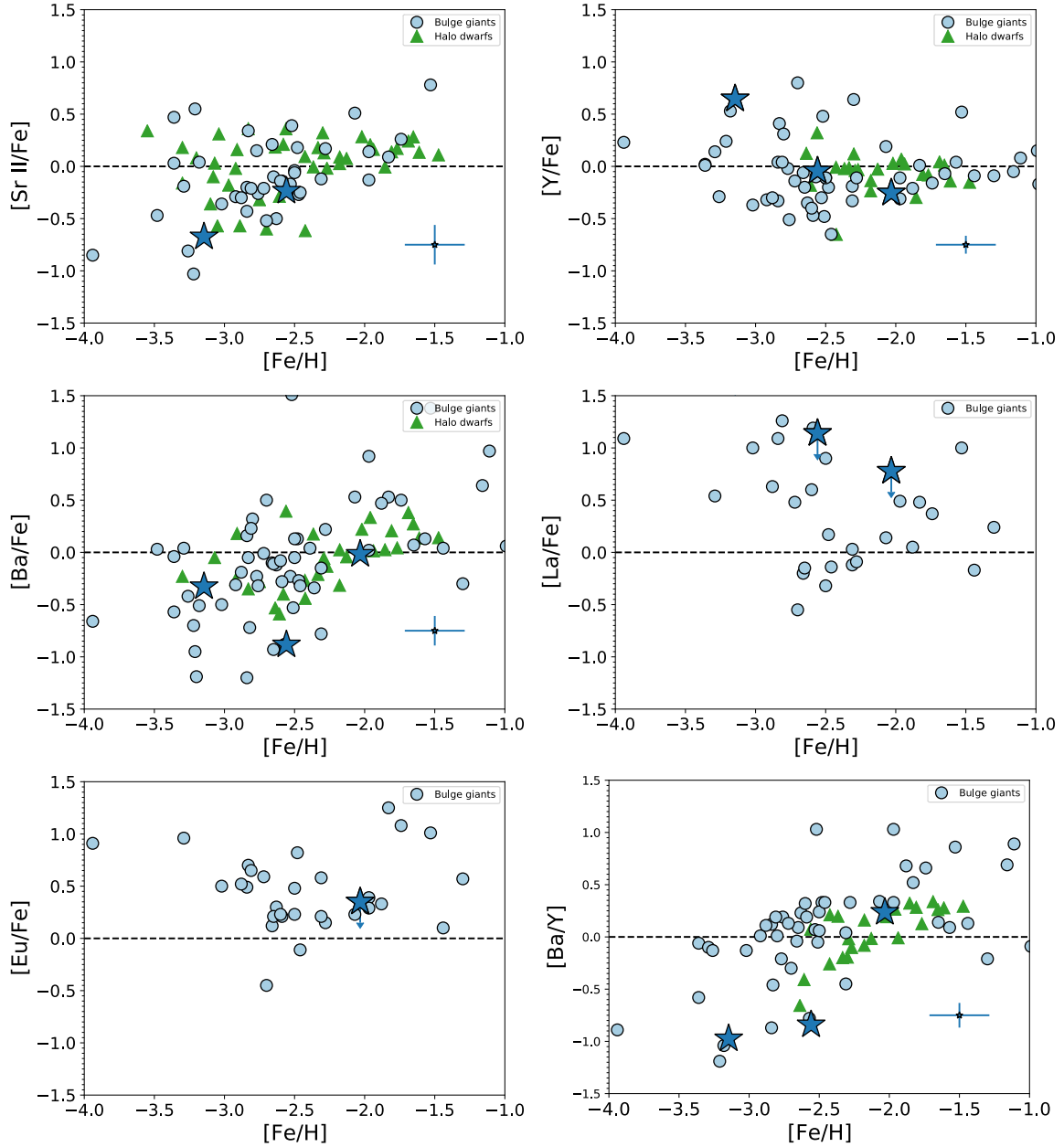


Figure 8. Abundances of neutron-capture elements strontium, yttrium, barium, lanthanum, and europium. We plot as blue stars our three metal-poor inner bulge giants. We plot as light blue circles a literature compilation of metal-poor outer bulge stars from [García Pérez et al. \(2013\)](#), [Casey & Schlafman \(2015\)](#), [Howes et al. \(2015, 2016\)](#), [Lamb et al. \(2017\)](#), and [Lucey et al. \(2019\)](#). We plot as light green squares halo giants from [Cayrel et al. \(2004\)](#) and as dark green triangles halo dwarfs from [Bonifacio et al. \(2009a\)](#) & [Reggiani et al. \(2017\)](#). The point with error bars in the bottom right of each panel corresponds to the mean uncertainty of our three stars. We find that the neutron-capture abundances of the inner and outer bulge are consistent with those in the halo.

focus only on the iron-peak abundances of chromium, manganese, cobalt, and nickel we find that the pure deflagration model “N100Hdef” from Fink et al. (2014) provides the best match to the abundances of 2MASS J175836.79-313707.6. The observable properties of model N100Hdef do not match those of any known class of Type Ia supernovae though. If instead we consider both the abundances of silicon and the iron-peak elements chromium, manganese, cobalt, and nickel we find that the DDT model “N1600C” from Seitenzahl et al. (2013b) with a compact, spherically symmetric ignition provides the best match to the abundances of 2MASS J175836.79-313707.6. In addition, model N1600C produces $[\text{Si}/\text{Mg}] \approx +0.9$ that is fully consistent with $[\text{Si}/\text{Mg}] \approx +0.6 \pm 0.3$ observed in 2MASS J175836.79-313707.6. Moreover, the observable properties of the DDT models from Seitenzahl et al. (2013b) do seem to match the properties of ordinary Type Ia supernovae. The sub-Chandrasekhar-mass model is a poor fit to the abundances of 2MASS J175836.79-313707.6.

We also compare the abundances of 2MASS J175836.79-313707.6 to the grid of updated Pop III core-collapse supernovae “znuc2012” models from Heger & Woosley (2010) using STARFIT¹⁵. Though the best fit model ($M_* = 10.9 M_\odot$, $KE_{\text{exp}} = 0.6$ B, $\log f_{\text{mix}} = -0.6$) has a similar χ^2 value as our preferred Chandrasekhar-mass thermonuclear model, it has an implausibly large amount of mixing and cannot explain the chromium, manganese, cobalt, or nickel abundances of 2MASS J175836.79-313707.6. Indeed, the similar χ^2 comes from the core-collapse model’s higher predicted cobalt yield that still fails to explain the cobalt abundance of 2MASS J175836.79-313707.6. Though the overall χ^2 values are comparable, we prefer the Chandrasekhar-mass thermonuclear supernovae model because it can self-consistently reproduce the chromium, manganese, iron, and nickel abundances of 2MASS J175836.79-313707.6. We plot in Figure 9 the best fit Chandrasekhar-mass and sub-Chandrasekhar-mass thermonuclear supernovae models along with the best-fit core-collapse supernova model.

Our scenario for the nucleosynthesis of the iron-peak elements in 2MASS J175836.79-313707.6 requires a Chandrasekhar-mass thermonuclear supernovae to occur about 10 Myr after the formation of the first stars in what would become the bulge of the Milky Way. Chandrasekhar-mass thermonuclear supernovae are often assumed to have occurred through the so-called “single degenerate” channel in which a CO white dwarf ac-

cretes material from Roche-lobe overflow or a strong wind from a main sequence, subgiant, helium star, or red giant binary companion. A single-degenerate Chandrasekhar-mass thermonuclear supernovae requires a CO white dwarf. At solar metallicity, the first CO white dwarfs appear 30 to 40 Myr after the onset of star formation when stars less massive than $8 M_\odot$ start to end their lives as white dwarfs. Metal-poor stars both move through their stellar evolution more quickly and produce more massive CO white dwarfs that require less accretion and therefore less time to reach the Chandrasekhar mass than solar-metallicity stars (e.g., Meng et al. 2008). The titanium abundance of 2MASS J175836.79-313707.6 prefers accretion from a helium star companion, and such configurations have been shown to reduce the delay times of thermonuclear supernovae (e.g., Wang et al. 2009a,b). As a result, it seems plausible that Chandrasekhar-mass thermonuclear supernovae delay times as short as 10 Myr might be achieved in a stellar population with $[\text{Fe}/\text{H}] \sim -3$.

Appealing to a thermonuclear supernova model that produces $0.5 M_\odot$ of iron to explain the iron-peak abundances of a star with $[\text{Fe}/\text{H}] = -3.15$ requires either a significant outflow of iron or an enormous dilution by unenriched gas. The depth of the potential at the center of the nascent Milky Way combined with the presence of dense gas fueling ongoing star formation that would shock ejecta and remove its kinetic energy indicates that dilution is a better explanation. To dilute $0.5 M_\odot$ of iron to the metallicity of 2MASS J175836.79-313707.6 requires mixing with about $10^6 M_\odot$ of pristine gas. While this is a substantial amount of unenriched gas, the young bulge is predicted to have had high accretions rates of pristine gas due to the high gas densities and frequent mergers expected for a relatively high σ peak in the redshift $z \gtrsim 2$ Universe.

The bulge of the young Milky Way is the ideal place to form stars like 2MASS J175836.79-313707.6. Even if the progenitor system of a Chandrasekhar-mass thermonuclear supernova that explodes with a delay time of 10 Myr is intrinsically rare, the star formation rate is so high in the bulge of the young Milky Way that there are lots of chances for it to form. The high star formation rate will also fully sample the stellar initial mass function and produce the massive Pop III or extreme Pop II stars necessary to produce the oxygen that will be transformed into silicon and scandium by future massive stars and their supernovae. The gas density and frequent mergers expected above $z \approx 2$ will provide the unenriched gas necessary to form stars with $[\text{Fe}/\text{H}] \sim -3$ in a region with a high star formation rate. We therefore suggest that stars with abundance

¹⁵ <http://starfit.org/>

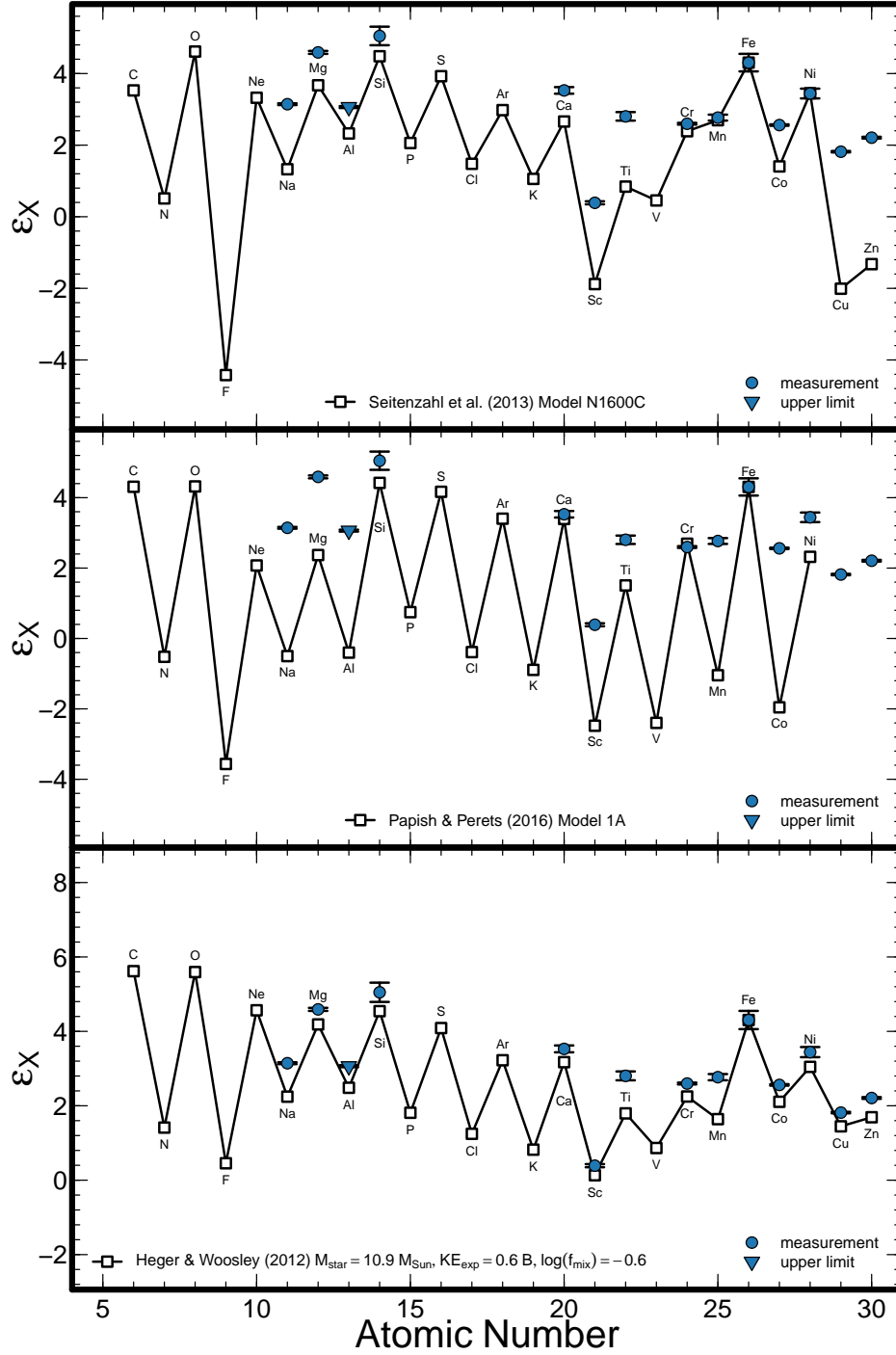


Figure 9. Comparison of our inferred abundances for 2MASS J175836.79-313707.6 with theoretical yields from supernovae models. We minimize χ^2 between our observed abundances and the thermonuclear supernovae and core-collapse supernovae yields predicted by Seitenzahl et al. (2013b), Fink et al. (2014), Ohlmann et al. (2014), Seitenzahl et al. (2016), Papish & Perets (2016), and an updated version of Heger & Woosley (2010) after fixing the predicted abundances patterns to match our inferred iron abundance. Top: when considering both silicon and the iron-peak elements chromium, manganese, cobalt, and nickel, we find that the Chandrasekhar-mass deflagration to detonation transition (DDT) model N1600C from Seitenzahl et al. (2013b) best reproduces our data. Middle: the best-fit sub-Chandrasekhar-mass model “1A” from Papish & Perets (2016) is a poor fit to the abundances of 2MASS J175836.79-313707.6. Bottom: the best-fit core-collapse supernova model cannot reproduce the chromium, manganese, cobalt, or nickel abundances of 2MASS J175836.79-313707.6.

patterns like that of 2MASS J175836.79-313707.6 enriched by thermonuclear supernovae should only be observed in the halo or classical dwarf spheroidal galaxies at higher metallicities. Though uncommon, the abundance pattern of 2MASS J175836.79-313707.6 is not unique. [de los Reyes et al. \(2020\)](#) inferred manganese abundances for 161 giants in six classical dwarf spheroidal galaxies and found $[\text{Mn}/\text{Fe}]$ as high as our inferred value for 2MASS J175836.79-313707.6 in stars at approximately $-3.0 \lesssim [\text{Fe}/\text{H}] \lesssim -2.5$. They concluded that their observed abundances are indicative of Chandrasekhar-mass thermonuclear supernovae occurring at higher metallicities $-2 \lesssim [\text{Fe}/\text{H}] \lesssim -1$.

6. CONCLUSION

Metal-poor stars in the bulge on tightly bound orbits are thought to be the oldest stars in the Milky Way. We used the mid-infrared metal-poor star selection of [Schlaufman & Casey \(2014\)](#) to find the three most metal-poor stars known in the inner bulge. All three stars are on tightly bound orbits and confined to the bulge region. The detailed abundances of our two inner bulge giants with $[\text{Fe}/\text{H}] \gtrsim -3$ have high iron-peak abundances but are otherwise similar to metal-poor stars in the outer bulge and halo. Our most metal-poor star 2MASS J175836.79-313707.6 has high $[\text{Ti}/\text{Fe}]$, $[\text{Sc}/\text{Fe}]$, and iron-peak abundances. It also has super-solar $[\text{Mn}/\text{Fe}]$. We argue that it is a second-generation Pop II star that was enriched by both massive Pop III or first-generation Pop II stars and a Chandrasekhar-mass thermonuclear supernova accreting from a helium star companion that exploded with a delay time of about 10 Myr. We argue that stars like 2MASS J175836.79-313707.6 with $[\text{Fe}/\text{H}] \lesssim -3$ should be much more common in the bulge than in the halo or dwarf galaxies because of the young bulge's high star formation rate and frequent inflows of unenriched gas.

ACKNOWLEDGMENTS

We thank the anonymous referee for the insightful comments that helped us improve this paper. Andy Casey is the recipient of an Australian Research Council Discovery Early Career Award (DECRA 190100656) funded by the Australian Government. Alex Ji is supported by NASA through Hubble Fellowship grant HST-HF2-51393.001, awarded by the Space Telescope Science Institute, which is operated by the Association of Universities for Research in Astronomy, Inc., for NASA, under contract NAS5-26555. This work is based in part on observations made with the Spitzer Space Telescope, which is operated by the Jet Propulsion Laboratory, California Institute of Technology under a contract with NASA. This publication makes use of data products from the Two Micron All Sky Survey, which is a joint project of the University of Massachusetts and the Infrared Processing and Analysis Center/California Institute of Technology, funded by the National Aeronautics and Space Administration and the National Science Foundation. This research has made use of the NASA/IPAC Infrared Science Archive, which is funded by the National Aeronautics and Space Administration and operated by the California Institute of Technology. Based in part on data acquired through the Australian Astronomical Observatory, under programs A/2015A/107 and A/2016A/103 plus Prop. ID 2016A-0086 and 2016B-0081 (PI: K. Schlaufman). We acknowledge the traditional owners of the land on which the AAT stands, the Gamilaraay people, and pay our respects to elders past and present. This paper includes data gathered with the 6.5 m Magellan Telescopes located at Las Campanas Observatory, Chile. This work has made use of data from the European Space Agency (ESA) mission *Gaia* (<https://www.cosmos.esa.int/gaia>), processed by the *Gaia* Data Processing and Analysis Consortium (DPAC, <https://www.cosmos.esa.int/web/gaia/dpac/consortium>). Funding for the DPAC has been provided by national institutions, in particular the institutions participating in the *Gaia* Multilateral Agreement. The national facility capability for SkyMapper has been funded through ARC LIEF grant LE130100104 from the Australian Research Council, awarded to the University of Sydney, the Australian National University, Swinburne University of Technology, the University of Queensland, the University of Western Australia, the University of Melbourne, Curtin University of Technology, Monash University and the Australian Astronomical Observatory. SkyMapper is owned and operated by The Australian National University's Research School of Astronomy and Astrophysics. The survey data were processed and provided by the SkyMapper Team at ANU.

The SkyMapper node of the All-Sky Virtual Observatory (ASVO) is hosted at the National Computational Infrastructure (NCI). Development and support the SkyMapper node of the ASVO has been funded in part by Astronomy Australia Limited (AAL) and the Australian Government through the Commonwealth's Education Investment Fund (EIF) and National Collaborative Research Infrastructure Strategy (NCRIS), particularly the National eResearch Collaboration Tools and Resources (NeCTAR) and the Australian National Data Service Projects (ANDS). This publication makes use of data products from the *Wide-field Infrared Survey Explorer*, which is a joint project of the University of California, Los Angeles, and the Jet Propulsion Laboratory/California Institute of Technology, funded by the National Aeronautics and Space Administration. This research has made use of NASA's Astrophysics Data System. This research has made use of the SIMBAD database, operated at CDS, Strasbourg, France (Wenger

et al. 2000). This research has made use of the VizieR catalogue access tool, CDS, Strasbourg, France (DOI: 10.26093/cds/vizieR). The original description of the VizieR service was published in 2000, A&AS 143, 23 (Ochsenbein et al. 2000).

Facilities: AAT (2dF + AAOmega), CTIO:2MASS, Magellan:Clay (MIKE echelle spectrograph), IRSA, Skymapper, Spitzer (IRAC), WISE.

Software: `astropy` (Astropy Collaboration et al. 2013, 2018), `CarPy` (Kelson et al. 2000; Kelson 2003), `galpy` (Bovy 2015), `q2` (Ramírez et al. 2014), `isochrones` (Morton 2015), `numpy` (van der Walt et al. 2011), `MultiNest` (Feroz & Hobson 2008; Feroz et al. 2009, 2019), `pandas` (Wes McKinney 2010), `R` (R Core Team 2020), `scipy` (Virtanen et al. 2020) `IRAF` (Tody 1986, 1993)

REFERENCES

- Amarsi, A. M., & Asplund, M. 2017, MNRAS, 464, 264, doi: [10.1093/mnras/stw2445](https://doi.org/10.1093/mnras/stw2445)
- Amarsi, A. M., Lind, K., Asplund, M., Barklem, P. S., & Collet, R. 2016, MNRAS, 463, 1518, doi: [10.1093/mnras/stw2077](https://doi.org/10.1093/mnras/stw2077)
- Andrievsky, S. M., Spite, M., Korotin, S. A., et al. 2007, A&A, 464, 1081, doi: [10.1051/0004-6361:20066232](https://doi.org/10.1051/0004-6361:20066232)
- Arenou, F., Luri, X., Babusiaux, C., et al. 2018, A&A, 616, A17, doi: [10.1051/0004-6361/201833234](https://doi.org/10.1051/0004-6361/201833234)
- Arentsen, A., Starkenburg, E., Martin, N. F., et al. 2020, MNRAS, 491, L11, doi: [10.1093/mnrasl/slz156](https://doi.org/10.1093/mnrasl/slz156)
- Asplund, M., Grevesse, N., Sauval, A. J., & Scott, P. 2009, ARA&A, 47, 481, doi: [10.1146/annurev.astro.46.060407.145222](https://doi.org/10.1146/annurev.astro.46.060407.145222)
- Astropy Collaboration, Robitaille, T. P., Tollerud, E. J., et al. 2013, A&A, 558, A33, doi: [10.1051/0004-6361/201322068](https://doi.org/10.1051/0004-6361/201322068)
- Astropy Collaboration, Price-Whelan, A. M., Sipőcz, B. M., et al. 2018, AJ, 156, 123, doi: [10.3847/1538-3881/aabc4f](https://doi.org/10.3847/1538-3881/aabc4f)
- Bailer-Jones, C. A. L., Rybizki, J., Fouesneau, M., Mantelet, G., & Andrae, R. 2018, AJ, 156, 58, doi: [10.3847/1538-3881/aacb21](https://doi.org/10.3847/1538-3881/aacb21)
- Barbuy, B., Chiappini, C., & Gerhard, O. 2018, ARA&A, 56, 223, doi: [10.1146/annurev-astro-081817-051826](https://doi.org/10.1146/annurev-astro-081817-051826)
- Battistini, C., & Bensby, T. 2016, A&A, 586, A49, doi: [10.1051/0004-6361/201527385](https://doi.org/10.1051/0004-6361/201527385)
- Baumüller, D., Butler, K., & Gehren, T. 1998, A&A, 338, 637
- Benjamin, R. A., Churchwell, E., Babler, B. L., et al. 2003, PASP, 115, 953, doi: [10.1086/376696](https://doi.org/10.1086/376696)
- Bensby, T., Feltzing, S., Gould, A., et al. 2017, A&A, 605, A89, doi: [10.1051/0004-6361/201730560](https://doi.org/10.1051/0004-6361/201730560)
- Bergemann, M., & Cescutti, G. 2010, A&A, 522, A9, doi: [10.1051/0004-6361/201014250](https://doi.org/10.1051/0004-6361/201014250)
- Bergemann, M., Gallagher, A. J., Eitner, P., et al. 2019, A&A, 631, A80, doi: [10.1051/0004-6361/201935811](https://doi.org/10.1051/0004-6361/201935811)
- Bernstein, R., Sheckman, S. A., Gunnels, S. M., Mochnacki, S., & Athey, A. E. 2003, in Society of Photo-Optical Instrumentation Engineers (SPIE) Conference Series, Vol. 4841, Proc. SPIE, ed. M. Iye & A. F. M. Moorwood, 1694–1704, doi: [10.1117/12.461502](https://doi.org/10.1117/12.461502)
- Blanco-Cuaresma, S. 2019, MNRAS, 486, 2075, doi: [10.1093/mnras/stz549](https://doi.org/10.1093/mnras/stz549)
- Blanco-Cuaresma, S., Soubiran, C., Heiter, U., & Jofré, P. 2014, A&A, 569, A111, doi: [10.1051/0004-6361/201423945](https://doi.org/10.1051/0004-6361/201423945)
- Bland-Hawthorn, J., & Gerhard, O. 2016, ARA&A, 54, 529, doi: [10.1146/annurev-astro-081915-023441](https://doi.org/10.1146/annurev-astro-081915-023441)
- Bonifacio, P., Spite, M., Cayrel, R., et al. 2009a, A&A, 501, 519, doi: [10.1051/0004-6361/200810610](https://doi.org/10.1051/0004-6361/200810610)
- . 2009b, A&A, 501, 519, doi: [10.1051/0004-6361/200810610](https://doi.org/10.1051/0004-6361/200810610)
- Bovy, J. 2015, ApJS, 216, 29, doi: [10.1088/0067-0049/216/2/29](https://doi.org/10.1088/0067-0049/216/2/29)
- Brook, C. B., Kawata, D., Scannapieco, E., Martel, H., & Gibson, B. K. 2007, ApJ, 661, 10, doi: [10.1086/511514](https://doi.org/10.1086/511514)

- Casagrande, L., Ramírez, I., Meléndez, J., Bessell, M., & Asplund, M. 2010, *A&A*, 512, A54, doi: [10.1051/0004-6361/200913204](https://doi.org/10.1051/0004-6361/200913204)
- Casey, A. R. 2016, *ApJS*, 223, 8, doi: [10.3847/0067-0049/223/1/8](https://doi.org/10.3847/0067-0049/223/1/8)
- Casey, A. R., & Schlafman, K. C. 2015, *ApJ*, 809, 110, doi: [10.1088/0004-637X/809/2/110](https://doi.org/10.1088/0004-637X/809/2/110)
- . 2017, *ApJ*, 850, 179, doi: [10.3847/1538-4357/aa9079](https://doi.org/10.3847/1538-4357/aa9079)
- Castelli, F., & Kurucz, R. L. 2004, arXiv Astrophysics e-prints
- Cayrel, R., Depagne, E., Spite, M., et al. 2004, *A&A*, 416, 1117, doi: [10.1051/0004-6361:20034074](https://doi.org/10.1051/0004-6361:20034074)
- Cescutti, G., François, P., Matteucci, F., Cayrel, R., & Spite, M. 2006, *A&A*, 448, 557, doi: [10.1051/0004-6361:20053622](https://doi.org/10.1051/0004-6361:20053622)
- Chieffi, A., & Limongi, M. 2004, *ApJ*, 608, 405, doi: [10.1086/392523](https://doi.org/10.1086/392523)
- Churchwell, E., Babler, B. L., Meade, M. R., et al. 2009, *PASP*, 121, 213, doi: [10.1086/597811](https://doi.org/10.1086/597811)
- Clayton, D. 2003, *Handbook of Isotopes in the Cosmos*
- Cunha, K., & Smith, V. V. 2006, *ApJ*, 651, 491, doi: [10.1086/507673](https://doi.org/10.1086/507673)
- de los Reyes, M. A. C., Kirby, E. N., Seitzzahl, I. R., & Shen, K. J. 2020, *ApJ*, 891, 85, doi: [10.3847/1538-4357/ab736f](https://doi.org/10.3847/1538-4357/ab736f)
- Diemand, J., Madau, P., & Moore, B. 2005, *MNRAS*, 364, 367, doi: [10.1111/j.1365-2966.2005.09604.x](https://doi.org/10.1111/j.1365-2966.2005.09604.x)
- Dotter, A., Chaboyer, B., Jevremović, D., et al. 2007, *AJ*, 134, 376, doi: [10.1086/517915](https://doi.org/10.1086/517915)
- . 2008, *ApJS*, 178, 89, doi: [10.1086/589654](https://doi.org/10.1086/589654)
- Eitner, P., Bergemann, M., Hansen, C. J., et al. 2020, *A&A*, 635, A38, doi: [10.1051/0004-6361/201936603](https://doi.org/10.1051/0004-6361/201936603)
- Feroz, F., & Hobson, M. P. 2008, *MNRAS*, 384, 449, doi: [10.1111/j.1365-2966.2007.12353.x](https://doi.org/10.1111/j.1365-2966.2007.12353.x)
- Feroz, F., Hobson, M. P., & Bridges, M. 2009, *MNRAS*, 398, 1601, doi: [10.1111/j.1365-2966.2009.14548.x](https://doi.org/10.1111/j.1365-2966.2009.14548.x)
- Feroz, F., Hobson, M. P., Cameron, E., & Pettitt, A. N. 2019, *The Open Journal of Astrophysics*, 2, 10, doi: [10.21105/astro.1306.2144](https://doi.org/10.21105/astro.1306.2144)
- Fink, M., Kromer, M., Seitzzahl, I. R., et al. 2014, *MNRAS*, 438, 1762, doi: [10.1093/mnras/stt2315](https://doi.org/10.1093/mnras/stt2315)
- Frebel, A., Casey, A. R., Jacobson, H. R., & Yu, Q. 2013, *ApJ*, 769, 57, doi: [10.1088/0004-637X/769/1/57](https://doi.org/10.1088/0004-637X/769/1/57)
- Gaia Collaboration, Prusti, T., de Bruijne, J. H. J., et al. 2016, *A&A*, 595, A1, doi: [10.1051/0004-6361/201629272](https://doi.org/10.1051/0004-6361/201629272)
- Gaia Collaboration, Brown, A. G. A., Vallenari, A., et al. 2018, *A&A*, 616, A1, doi: [10.1051/0004-6361/201833051](https://doi.org/10.1051/0004-6361/201833051)
- Gao, L., Theuns, T., Frenk, C. S., et al. 2010, *MNRAS*, 403, 1283, doi: [10.1111/j.1365-2966.2009.16225.x](https://doi.org/10.1111/j.1365-2966.2009.16225.x)
- García Pérez, A. E., Cunha, K., Shetrone, M., et al. 2013, *ApJL*, 767, L9, doi: [10.1088/2041-8205/767/1/L9](https://doi.org/10.1088/2041-8205/767/1/L9)
- Gargiulo, I. D., Cora, S. A., Vega-Martínez, C. A., et al. 2017, *MNRAS*, 472, 4133, doi: [10.1093/mnras/stx2188](https://doi.org/10.1093/mnras/stx2188)
- Gonzalez, O. A., Rejkuba, M., Zoccali, M., Valenti, E., & Minniti, D. 2011, *A&A*, 534, A3, doi: [10.1051/0004-6361/201117601](https://doi.org/10.1051/0004-6361/201117601)
- Gonzalez, O. A., Rejkuba, M., Zoccali, M., et al. 2012, *A&A*, 543, A13, doi: [10.1051/0004-6361/201219222](https://doi.org/10.1051/0004-6361/201219222)
- Gravity Collaboration, Abuter, R., Amorim, A., et al. 2018, *A&A*, 615, L15, doi: [10.1051/0004-6361/201833718](https://doi.org/10.1051/0004-6361/201833718)
- Griffen, B. F., Dooley, G. A., Ji, A. P., et al. 2018, *MNRAS*, 474, 443, doi: [10.1093/mnras/stx2749](https://doi.org/10.1093/mnras/stx2749)
- Grimmett, J. J., Karakas, A. I., Heger, A., & Müller, B. 2019, arXiv e-prints, arXiv:1911.05901, <https://arxiv.org/abs/1911.05901>
- Gustafsson, B., Edvardsson, B., Eriksson, K., et al. 2008, *A&A*, 486, 951, doi: [10.1051/0004-6361:200809724](https://doi.org/10.1051/0004-6361:200809724)
- Hambly, N. C., Cropper, M., Boudreault, S., et al. 2018, *A&A*, 616, A15, doi: [10.1051/0004-6361/201832716](https://doi.org/10.1051/0004-6361/201832716)
- Hansen, C. J., Bergemann, M., Cescutti, G., et al. 2013, *A&A*, 551, A57, doi: [10.1051/0004-6361/201220584](https://doi.org/10.1051/0004-6361/201220584)
- Heger, A., & Woosley, S. E. 2010, *ApJ*, 724, 341, doi: [10.1088/0004-637X/724/1/341](https://doi.org/10.1088/0004-637X/724/1/341)
- Howes, L. M., Casey, A. R., Asplund, M., et al. 2015, *Nature*, 527, 484, doi: [10.1038/nature15747](https://doi.org/10.1038/nature15747)
- Howes, L. M., Asplund, M., Keller, S. C., et al. 2016, *MNRAS*, 460, 884, doi: [10.1093/mnras/stw1004](https://doi.org/10.1093/mnras/stw1004)
- Ishiyama, T., Sudo, K., Yokoi, S., et al. 2016, *ApJ*, 826, 9, doi: [10.3847/0004-637X/826/1/9](https://doi.org/10.3847/0004-637X/826/1/9)
- Jacobson, H. R., & Friel, E. D. 2013, *AJ*, 145, 107, doi: [10.1088/0004-6256/145/4/107](https://doi.org/10.1088/0004-6256/145/4/107)
- Ji, A. P., Frebel, A., Chiti, A., & Simon, J. D. 2016, *Nature*, 531, 610, doi: [10.1038/nature17425](https://doi.org/10.1038/nature17425)
- Johnson, C. I., Rich, R. M., Kobayashi, C., & Fulbright, J. P. 2012, *ApJ*, 749, 175, doi: [10.1088/0004-637X/749/2/175](https://doi.org/10.1088/0004-637X/749/2/175)
- Jurić, M., Ivezić, Ž., Brooks, A., et al. 2008, *ApJ*, 673, 864, doi: [10.1086/523619](https://doi.org/10.1086/523619)
- Kelson, D. D. 2003, *PASP*, 115, 688, doi: [10.1086/375502](https://doi.org/10.1086/375502)
- Kelson, D. D., Illingworth, G. D., van Dokkum, P. G., & Franx, M. 2000, *ApJ*, 531, 159, doi: [10.1086/308445](https://doi.org/10.1086/308445)
- Kelson, D. D., Williams, R. J., Dressler, A., et al. 2014, *ApJ*, 783, 110, doi: [10.1088/0004-637X/783/2/110](https://doi.org/10.1088/0004-637X/783/2/110)
- Kobayashi, C., Umeda, H., Nomoto, K., Tominaga, N., & Ohkubo, T. 2006, *ApJ*, 653, 1145, doi: [10.1086/508914](https://doi.org/10.1086/508914)
- Korn, A. J., Shi, J., & Gehren, T. 2003, *A&A*, 407, 691, doi: [10.1051/0004-6361:20030907](https://doi.org/10.1051/0004-6361:20030907)
- Lamb, M., Venn, K., Andersen, D., et al. 2017, *MNRAS*, 465, 3536, doi: [10.1093/mnras/stw2865](https://doi.org/10.1093/mnras/stw2865)

- Lind, K., Asplund, M., Barklem, P. S., & Belyaev, A. K. 2011, *A&A*, 528, A103, doi: [10.1051/0004-6361/201016095](https://doi.org/10.1051/0004-6361/201016095)
- Lindgren, L., Hernández, J., Bombrun, A., et al. 2018, *A&A*, 616, A2, doi: [10.1051/0004-6361/201832727](https://doi.org/10.1051/0004-6361/201832727)
- Livne, E., & Arnett, D. 1995, *ApJ*, 452, 62, doi: [10.1086/176279](https://doi.org/10.1086/176279)
- Lucey, M., Hawkins, K., Ness, M., et al. 2019, *MNRAS*, 488, 2283, doi: [10.1093/mnras/stz1847](https://doi.org/10.1093/mnras/stz1847)
- Luri, X., Brown, A. G. A., Sarro, L. M., et al. 2018, *A&A*, 616, A9, doi: [10.1051/0004-6361/201832964](https://doi.org/10.1051/0004-6361/201832964)
- Mainzer, A., Grav, T., Bauer, J., et al. 2011, *ApJ*, 743, 156, doi: [10.1088/0004-637X/743/2/156](https://doi.org/10.1088/0004-637X/743/2/156)
- Mashonkina, L. I., & Belyaev, A. K. 2019, *Astronomy Letters*, 45, 341, doi: [10.1134/S1063773719060033](https://doi.org/10.1134/S1063773719060033)
- Meng, X., Chen, X., & Han, Z. 2008, *A&A*, 487, 625, doi: [10.1051/0004-6361:20078841](https://doi.org/10.1051/0004-6361:20078841)
- Miyamoto, M., & Nagai, R. 1975, *PASJ*, 27, 533
- Morton, T. D. 2015, *isochrones: Stellar model grid package*. <http://ascl.net/1503.010>
- Mucciarelli, A., & Bonifacio, P. 2020, *arXiv e-prints*, arXiv:2003.07390. <https://arxiv.org/abs/2003.07390>
- Navarro, J. F., Frenk, C. S., & White, S. D. M. 1996, *ApJ*, 462, 563, doi: [10.1086/177173](https://doi.org/10.1086/177173)
- Ness, M., Freeman, K., Athanassoula, E., et al. 2013, *MNRAS*, 430, 836, doi: [10.1093/mnras/sts629](https://doi.org/10.1093/mnras/sts629)
- Nishiyama, S., Tamura, M., Hatano, H., et al. 2009, *ApJ*, 696, 1407, doi: [10.1088/0004-637X/696/2/1407](https://doi.org/10.1088/0004-637X/696/2/1407)
- Ochsenbein, F., Bauer, P., & Marcout, J. 2000, *A&AS*, 143, 23, doi: [10.1051/aas:2000169](https://doi.org/10.1051/aas:2000169)
- Ohlmann, S. T., Kromer, M., Fink, M., et al. 2014, *A&A*, 572, A57, doi: [10.1051/0004-6361/201423924](https://doi.org/10.1051/0004-6361/201423924)
- Papish, O., & Perets, H. B. 2016, *ApJ*, 822, 19, doi: [10.3847/0004-637X/822/1/19](https://doi.org/10.3847/0004-637X/822/1/19)
- Queiroz, A. B. A., Anders, F., Santiago, B. X., et al. 2018, *MNRAS*, 476, 2556, doi: [10.1093/mnras/sty330](https://doi.org/10.1093/mnras/sty330)
- Queiroz, A. B. A., Anders, F., Chiappini, C., et al. 2020, *A&A*, 638, A76, doi: [10.1051/0004-6361/201937364](https://doi.org/10.1051/0004-6361/201937364)
- R Core Team. 2020, *R: A Language and Environment for Statistical Computing*, R Foundation for Statistical Computing, Vienna, Austria. <https://www.R-project.org/>
- Ramírez, I., Meléndez, J., Bean, J., et al. 2014, *A&A*, 572, A48, doi: [10.1051/0004-6361/201424244](https://doi.org/10.1051/0004-6361/201424244)
- Reggiani, H., Meléndez, J., Kobayashi, C., Karakas, A., & Placco, V. 2017, *A&A*, 608, A46, doi: [10.1051/0004-6361/201730750](https://doi.org/10.1051/0004-6361/201730750)
- Roederer, I. U., Preston, G. W., Thompson, I. B., et al. 2014, *AJ*, 147, 136, doi: [10.1088/0004-6256/147/6/136](https://doi.org/10.1088/0004-6256/147/6/136)
- Salvadori, S., Ferrara, A., Schneider, R., Scannapieco, E., & Kawata, D. 2010, *MNRAS*, 401, L5, doi: [10.1111/j.1745-3933.2009.00772.x](https://doi.org/10.1111/j.1745-3933.2009.00772.x)
- Scannapieco, E., Kawata, D., Brook, C. B., et al. 2006, *ApJ*, 653, 285, doi: [10.1086/508487](https://doi.org/10.1086/508487)
- Schlafman, K. C., & Casey, A. R. 2014, *ApJ*, 797, 13, doi: [10.1088/0004-637X/797/1/13](https://doi.org/10.1088/0004-637X/797/1/13)
- Seitzzahl, I. R., Cescutti, G., Röpke, F. K., Ruiter, A. J., & Pakmor, R. 2013a, *A&A*, 559, L5, doi: [10.1051/0004-6361/201322599](https://doi.org/10.1051/0004-6361/201322599)
- Seitzzahl, I. R., & Townsley, D. M. 2017, *Nucleosynthesis in Thermonuclear Supernovae*, ed. A. W. Alsabti & P. Murdin, 1955, doi: [10.1007/978-3-319-21846-5_87](https://doi.org/10.1007/978-3-319-21846-5_87)
- Seitzzahl, I. R., Ciaraldi-Schoolmann, F., Röpke, F. K., et al. 2013b, *MNRAS*, 429, 1156, doi: [10.1093/mnras/sts402](https://doi.org/10.1093/mnras/sts402)
- Seitzzahl, I. R., Kromer, M., Ohlmann, S. T., et al. 2016, *A&A*, 592, A57, doi: [10.1051/0004-6361/201527251](https://doi.org/10.1051/0004-6361/201527251)
- Sharma, M., Theuns, T., & Frenk, C. 2018, *MNRAS*, 479, 1638, doi: [10.1093/mnras/sty1319](https://doi.org/10.1093/mnras/sty1319)
- Shectman, S. A., & Johns, M. 2003, in *Society of Photo-Optical Instrumentation Engineers (SPIE) Conference Series*, Vol. 4837, Proc. SPIE, ed. J. M. Oschmann & L. M. Stepp, 910–918, doi: [10.1117/12.457909](https://doi.org/10.1117/12.457909)
- Singh, D., Hansen, C. J., Byrgesen, J. S., Reichert, M., & Reggiani, H. M. 2020, *A&A*, 634, A72, doi: [10.1051/0004-6361/201936305](https://doi.org/10.1051/0004-6361/201936305)
- Skrutskie, M. F., Cutri, R. M., Stiening, R., et al. 2006, *AJ*, 131, 1163, doi: [10.1086/498708](https://doi.org/10.1086/498708)
- Snedden, C., Lawler, J. E., Cowan, J. J., Ivans, I. I., & Den Hartog, E. A. 2009, *ApJS*, 182, 80, doi: [10.1088/0067-0049/182/1/80](https://doi.org/10.1088/0067-0049/182/1/80)
- Snedden, C., Lawler, J. E., den Hartog, E. A., & Wood, M. E. 2016, *IAU Focus Meeting*, 29A, 287, doi: [10.1017/S1743921316003069](https://doi.org/10.1017/S1743921316003069)
- Snedden, C. A. 1973, PhD thesis, THE UNIVERSITY OF TEXAS AT AUSTIN.
- Starkenburg, E., Oman, K. A., Navarro, J. F., et al. 2017, *MNRAS*, 465, 2212, doi: [10.1093/mnras/stw2873](https://doi.org/10.1093/mnras/stw2873)
- Tody, D. 1986, *Society of Photo-Optical Instrumentation Engineers (SPIE) Conference Series*, Vol. 627, *The IRAF Data Reduction and Analysis System*, ed. D. L. Crawford, 733, doi: [10.1117/12.968154](https://doi.org/10.1117/12.968154)
- . 1993, *Astronomical Society of the Pacific Conference Series*, Vol. 52, *IRAF in the Nineties*, ed. R. J. Hanisch, R. J. V. Brissenden, & J. Barnes, 173
- Tumlinson, J. 2010, *ApJ*, 708, 1398, doi: [10.1088/0004-637X/708/2/1398](https://doi.org/10.1088/0004-637X/708/2/1398)

- van der Walt, S., Colbert, S. C., & Varoquaux, G. 2011, Computing in Science and Engineering, 13, 22, doi: [10.1109/MCSE.2011.37](https://doi.org/10.1109/MCSE.2011.37)
- Virtanen, P., Gommers, R., Oliphant, T. E., et al. 2020, Nature Methods, 17, 261, doi: <https://doi.org/10.1038/s41592-019-0686-2>
- Wang, B., Chen, X., Meng, X., & Han, Z. 2009a, ApJ, 701, 1540, doi: [10.1088/0004-637X/701/2/1540](https://doi.org/10.1088/0004-637X/701/2/1540)
- Wang, B., Meng, X., Chen, X., & Han, Z. 2009b, MNRAS, 395, 847, doi: [10.1111/j.1365-2966.2009.14545.x](https://doi.org/10.1111/j.1365-2966.2009.14545.x)
- Wenger, M., Ochsenbein, F., Egret, D., et al. 2000, A&AS, 143, 9, doi: [10.1051/aas:2000332](https://doi.org/10.1051/aas:2000332)
- Wes McKinney. 2010, in Proceedings of the 9th Python in Science Conference, ed. Stéfan van der Walt & Jarrod Millman, 56 – 61, doi: [10.25080/Majora-92bf1922-00a](https://doi.org/10.25080/Majora-92bf1922-00a)
- Wolf, C., Onken, C. A., Luvaul, L. C., et al. 2018, PASA, 35, e010, doi: [10.1017/pasa.2018.5](https://doi.org/10.1017/pasa.2018.5)
- Woolley, S. E., & Weaver, T. A. 1994, ApJ, 423, 371, doi: [10.1086/173813](https://doi.org/10.1086/173813)
- . 1995, ApJS, 101, 181, doi: [10.1086/192237](https://doi.org/10.1086/192237)
- Wright, E. L. 2006, PASP, 118, 1711, doi: [10.1086/510102](https://doi.org/10.1086/510102)
- Wright, E. L., Eisenhardt, P. R. M., Mainzer, A. K., et al. 2010, AJ, 140, 1868, doi: [10.1088/0004-6256/140/6/1868](https://doi.org/10.1088/0004-6256/140/6/1868)
- Yamaguchi, H., Badenes, C., Foster, A. R., et al. 2015, ApJL, 801, L31, doi: [10.1088/2041-8205/801/2/L31](https://doi.org/10.1088/2041-8205/801/2/L31)